Am J Physiol Cell Physiol 293: C815–C829, 2007.
First published; doi:10.1152/ajpcell.00355.2006.

Adenine nucleotide-creatine-phosphate module in myocardial metabolic system explains fast phase of dynamic regulation of oxidative phosphorylation

Johannes H. G. M. van Beek

Data Integration, Analysis and Logistics (DIAL) Project, Centre for Medical Systems Biology, Leiden, Rotterdam, and Amsterdam; and VU University Medical Centre, Amsterdam, The Netherlands

Submitted 27 June 2006; accepted in final form 13 June 2007

van Beek JH. Adenine nucleotide-creatine-phosphate module in myocardial metabolic system explains fast phase of dynamic regulation of oxidative phosphorylation. *Am J Physiol Cell Physiol* 293: C815–C829, 2007. First published; doi:10.1152/ajpcell.00355.2006.—Computational models of a large metabolic system can be assembled from modules that represent a biological function emerging from interaction of a small subset of molecules. A "skeleton model" is tested here for a module that regulates the first phase of dynamic adaptation of oxidative phosphorylation (OxPhos) to demand in heart muscle cells. The model contains only diffusion, mitochondrial outer membrane (MOM) permeation, and two isoforms of creatine kinase (CK), in cytosol and mitochondrial intermembrane space (IMS), respectively. The communication with two neighboring modules occurs via stimulation of mitochondrial ATP production by ADP and P_i from the IMS and via time-varying cytosolic ATP hydrolysis during contraction. Assuming normal cytosolic diffusion and high MOM permeability for ADP, the response time of OxPhos (t_{mito}; generalized time constant) to steps in cardiac pacing rate is predicted to be 2.4 s. In contrast, with low MOM permeability, t_{mito} is predicted to be 15 s. An optimized MOM permeability of 21 μm/s gives t_{mito} = 3.7 s, in agreement with experiments on rabbit heart with blocked glycolytic ATP synthesis. The model correctly predicts a lower t_{mito} if CK activity is reduced by 98%. Among others, the following predictions result from the model analysis: *1*) CK activity buffers large ADP oscillations; *2*) ATP production is pulsatile in beating heart, although it adapts slowly to demand with "time constant" ~14 heartbeats; *3*) if the muscle isoform of CK is overexpressed, OxPhos reacts slower to changing workload; and *4*) if mitochondrial CK is overexpressed, OxPhos reacts faster.

systems biology; computational model; creatine kinase; phosphocreatine shuttle; regulatory module; mitochondrial membrane permeability; oxygen consumption

SYSTEMS BIOLOGY focuses on the biological function that emerges from interacting molecules in the biological system. This article examines one functional characteristic of heart muscle: the adaptation of ATP production by the mitochondria to the ATP hydrolysis, which is coupled to force development and mechanical pump work. Changing demands on the heart require that ATP production adapts quickly to ATP usage by myofibrils and ion pumps during contractile work.

To analyze the dynamic adaptation of cardiac ATP synthesis to ATP hydrolysis, a "skeleton model" approach was chosen, incorporating key elements of biochemical reaction and transport of phosphoryl groups in the muscle cell (29, 41). These key processes were chosen from the thousands of molecules at work in the cell and were hypothesized to form the core module that regulates the fast dynamic adaptation of oxidative phosphorylation (OxPhos) to ATP hydrolysis, which varies with the load on the heart. The model is simplified as much as possible.

A minimal requirement for resynthesis of ATP after its hydrolysis to ADP and P_i is that ADP and P_i are transferred to the mitochondria to serve as substrates for OxPhos. ATP can also be resynthesized from phosphocreatine (PCr) via isoforms of the creatine kinase (CK) enzyme. The high-energy phosphate groups of ATP synthesized in the mitochondria may be transferred to creatine to yield PCr, in a reaction catalyzed by the mitochondrial isoform of CK, Mi-CK, located in the mitochondrial intermembrane space (IMS). Phosphate group transfer between adenine nucleotide and creatine (Cr) on the one hand and transport of these metabolites between cytosol and IMS on the other constitute the adenine nucleotide-creatine-phosphate (ACP) module, which is the focus of the present study. It is investigated here whether this module can explain experimental results on the fast dynamic adaptation of OxPhos to ATP hydrolysis.

It was proposed that ADP and ATP are not transferred directly between cytosol and mitochondria under normal conditions, but instead there exists a more or less obligatory "PCr shuttle," which transfers the "high-energy" phosphoryl groups after phosphate group transfer from ATP to Cr in the mitochondrial intermembrane space (5, 42). In the myofibrils the phosphoryl group of PCr would then be transferred back to ATP by the muscular isoform of CK (MM-CK) to energize myofibrillar contraction. Conversely, creatine may then also be important in the intracellular signaling pathway, which regulates dynamic adaptation of OxPhos to changing ATP hydrolysis in the myofibrils and at ion pumps. The permeability of the mitochondrial outer membrane (MOM) to ADP and ATP is a key parameter determining the importance of the PCr shuttle.

The ACP module is computationally modeled to represent the time course and dynamics of the high-energy metabolites, which contain phosphate groups. Adjacent modules, which produce and consume ATP in exchange with the ACP module, are not described extensively. These modules are represented by relatively simple equations that summarize the functioning of the ATP splitting module in the cytosol and ATP production by the mitochondria. ATP exported from the mitochondria across the adenine nucleotide translocator in exchange for ADP together with the uptake of P_i across the mitochondrial inner membrane form the interface between the ACP module and the module for mitochondrial ATP production. The time course of ATP hydrolysis in the cytosol is given by a forcing function determined from experimental measurements.

Address for reprint requests and other correspondence: J. H. G. M. van Beek, Dept. of Molecular Cell Physiology, FALW, Vrije Universiteit, De Boelelaan 1085, 1081 HV Amsterdam (e-mail: hans.van.beek@falw.vu.nl).

The costs of publication of this article were defrayed in part by the payment of page charges. The article must therefore be hereby marked "*advertisement*" in accordance with 18 U.S.C. Section 1734 solely to indicate this fact.

The ACP module is investigated here by isolating it as much as possible experimentally. Cytosolic ATP production by glycolysis is inhibited chemically at the level of glyceraldehyde-3-phosphate dehydrogenase in the experiments used to test the model (17). Pyruvate is given as a carbon source for the mitochondria to bypass glycolysis. The response of OxPhos was shown to be about twice as slow when glycolysis is active (17). In the present study, the situation is investigated where glycolysis is inactive, both in the model and in the experiments.

In addition to ADP and P_i, the direct substrates for oxidative phosphorylation, and PCr and Cr as intermediates in phosphate group transfer, other factors have been proposed to regulate oxidative phosphorylation during work transitions. Intracellular Ca^{2+} was proposed as an important regulator, but it turns out that it stimulates OxPhos with a time constant of ~20–25 s, leading to increased NADH synthesis in a second, slow phase of the response (7). In contrast, the first phase of the response of OxPhos is characterized by a fast time constant of ~4 s, which is accompanied by enhanced NADH oxidation rather than reduction (7, 10). Therefore, the effect of Ca^{2+} stimulation on the mitochondria is omitted from the model because it only plays a role at a slower time scale.

Cardiac mitochondria are exposed to time-varying loads at two levels: pulsatile ATP hydrolysis occurs during systole and is low during diastole in the cardiac cycle (41, 45), and at a slower time scale heart rate varies. In the present study the model is tested by simulating the response to dynamic variations in ATP hydrolysis caused by heart rate steps and comparing the response time with experimental measurements. The role of CK is tested further by model simulation of the effect of lower CK activity on dynamic adaptation and comparing this with experimental results of inhibition of CK. The analysis demonstrates that the chemical reactions of ATP and ADP, with Cr and PCr, respectively, catalyzed by two CK isoforms which are linked by diffusion through the cytosol and permeation of the MOM are sufficient to explain the time course of dynamic adaptation of ATP synthesis to time-varying ATP hydrolysis.

METHODS

Description of the model. The ACP module contains the metabolites ATP, ADP, creatine (Cr), phosphocreatine (PCr), and P_i. The transport of these metabolites between the two compartments in the module, cytosol and mitochondrial intermembrane space, is represented by a diffusional conductance term. The module includes phosphate group transfer between creatine and adenine nucleotides catalyzed by MM-CK in the cytosol and by Mi-CK in the IMS (see Fig. 1). In the cytosolic compartment the ACP module exchanges ATP for ADP and P_i with an ATP hydrolysis module, and ADP and P_i from the IMS are exchanged for ATP with an ATP production module representing mitochondrial ATP synthesis. Communication with the latter two modules embeds the ACP module in the system. ATP can also be synthesized by glycolysis, but in the present study experiments are analyzed in which glycolysis had been inhibited and bypassed (17) and the model therefore does not include glycolysis. The kinetic equations for the ACP module and two communicating modules are given in APPENDIX A.

Central metabolites in the ACP module are ATP and its hydrolysis products ADP and P_i. ATP can be synthesized from PCr and ADP, forming Cr in a reaction catalyzed by CK. The CK reaction runs in both directions.

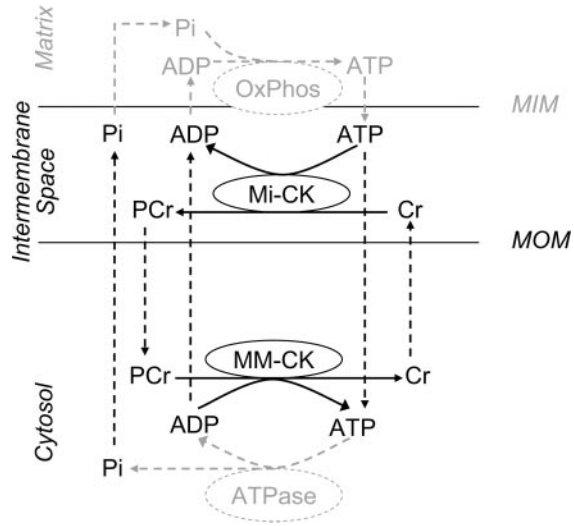

Fig. 1. Scheme of the adenine nucleotide-creatine-phosphate (ACP) module. Components of the ACP module are shown in black. Mitochondrial ATP production and the cytosolic ATPase catalyzing ATP hydrolysis are not considered to be part of the ACP module. These adjacent modules, which communicate with the ACP module, are shown in gray. The input to the ACP module is the ATP hydrolysis forcing function (ATPase), representing ATP splitting by contractile proteins and ion pumps. The hydrolyzed ATP is resynthesized in the mitochondrial matrix via oxidative phosphorylation (OxPhos) and exported across the mitochondrial inner membrane (MIM). The ATP production module communicates with the ACP module via uptake of P_i and exchange of ADP for ATP across the MIM. Concentration changes of ATP, ADP, and P_i are influenced by the reaction of ATP with creatine (Cr), yielding phosphocreatine (PCr) and ADP, catalyzed by isoforms of creatine kinase (CK) enzymes. CK has a muscular isoform (MM-CK) in the cytosol and a mitochondrial isoform (Mi-CK) in the mitochondrial intermembrane space. Note that P_i is not handled by CK and diffuses directly between the compartments without taking part in chemical reactions. PCr and Cr have higher diffusivity than the adenine nucleotides. The permeability to ADP and ATP of the outer mitochondrial membrane (MOM), which separates the compartments, may be restricted and is an important parameter varied in the model analysis.

$$ATP + Cr \leftrightarrow ADP + PCr \quad (1)$$

This is the only reaction to synthesize PCr, which helps to isolate the module from the rest of the system. The mitochondrial isoform of CK, Mi-CK, is located in the mitochondrial intermembrane space (see Fig. 1) and produces PCr from ATP in the IMS. The myofibrillar isoform of CK (MM-CK) catalyzes net production of ATP in the contractile elements of the muscle cell. Net synthesis of PCr by Mi-CK, followed by diffusion of PCr to MM-CK in the myofibrils where ATP is formed, constitutes a PCr shuttle (5).

ATP hydrolysis takes place in the myofibrils and at ion pumps during contraction, producing ADP plus P_i:

$$ATP \rightarrow ADP + P_i \quad (2)$$

The ATP hydrolysis module is represented by a forcing function giving the time course of ATP hydrolysis, determined from experimental measurements. CK buffers the ADP in the cytosol and myofibrils, keeping ADP levels low and ATP levels high. Adenylate kinase (AK) has been proposed to play a similar role as CK, but is omitted from the simplified ACP module because it quantitatively plays a minor role (23) and experiments on AK knockout mice show similar response times of OxPhos as controls with AK active (15).

Another major simplification is the omittance of special forms of functional coupling via a microcompartment between Mi-CK and the adenine nucleotide translocator (41). It is emphasized here that such special coupling may be important to explain measurements in iso-

lated mitochondria. However, several considerations argue for omitting the microcompartment. First, in isolated rabbit heart mitochondria the coupling strength was shown to be inversely proportional to ATP concentration and is very low for >0.7 mM ATP (14), a condition which exists in heart muscle cells. Second, simulations with the full model (41) and with the reduced model yield similar results irrespective of functional coupling (23). Restrictions in membrane permeability between IMS and cytosol allowed in the reduced model already lead to a limited form of functional coupling between Mi-CK and adenine nucleotide translocator. To preserve the "skeleton model" approach and limit the number of parameters, special forms of functional coupling are omitted from the model, although we reiterate that functional coupling may be important to explain studies on isolated mitochondria and skinned fibers (14, 21).

An assumption for the ATP production module is that the concentrations of ADP and P_i in the IMS are the only variables determining the rate of OxPhos. ATP production is given by a simple Michaelis-Menten-type equation as a function of the ADP and P_i concentrations (see APPENDIX A). This equation lumps the complex processes involving the mitochondrial adenine nucleotide translocator, mitochondrial matrix, inner membrane proton pumps, and electrical potential in a simple overall equation which has been tested extensively on isolated mitochondria (16, 36) and is used often for modeling (19, 25). The ATP production enters the IMS compartment of the ACP module as a flux of ATP exported from the mitochondrial matrix in exchange for ADP. The response of ATP production to ADP and P_i in the IMS is assumed to be instantaneous in the model. Experimental evidence shows that the mitochondrial response to ADP is fast as indicated by a measured half time of 0.07 s at 26°C for the response of cytochrome *b* in the electron transport chain to external ADP addition (9). Model simulations, which I performed with the model of Cortassa et al. (10), suggest that the response of ATP export from the mitochondrion into the intermembrane space in response to ADP concentration changes in the IMS at the adenine nucleotide translocator are very fast, <1 ms, while mitochondrial O_2 consumption follows with a response time of ~3 ms in this model simulation. ATP production (i.e., export from the mitochondrial matrix), ATP synthesis, OxPhos, and mitochondrial O_2 consumption are very closely coupled in time.

The ACP module is a simplification of the model of Vendelin et al. (41). In the original model, the transfer of energy was simulated by a spatially inhomogeneous reaction-diffusion process allowing for diffusion gradients in the cytosol, which were, however, shown to be very small in those simulations. The steps taken in simplification were discussed and the simplified model gave results which are very close to results of the extensive reaction-diffusion model in a preliminary analysis of this model presented at a conference (23).

Estimation of diffusion and membrane permeation parameters. In the model simulations use is made of estimates of conductance parameters for diffusion in the myofibrillar and cytosolic space and for permeation of the MOM, taking place in series. For the cytosol, the conductance parameter is calculated from diffusion coefficients measured from diffusion-sensitized NMR spectra in muscle (11) based on a cylindrical geometry of the myofibril and surrounding cytosolic space (see Table 2 and APPENDIX B, parameter set I).

The average diffusional transit time t_{diff} for a metabolite is defined by analogy to the mean transit time for a metabolized indicator, and is obtained by dividing the change in the amount of metabolite in the space through which the metabolite diffuses by the change in metabolic rate, which causes this change in amount (40) (see APPENDIX B). This t_{diff} for the myofibrillar space is 0.34 ms for ATP, 0.35 ms for ADP, 0.24 ms for PCr, 0.20 ms for Cr, and 0.19 ms for P_i. These diffusional transit times are a minute fraction of the response time of oxidative phosphorylation to changes in metabolism in the myofibrillar space. The diffusion gradients in the cytosolic compartment between myofibrillar core and MOM are established so quickly that they can be represented by a diffusion conductance in the model (see APPENDIX A and Table 2). This type of accurate approximation is often used in modeling, for instance by neglecting radial diffusion gradients in blood-tissue exchange models (3).

In addition to diffusion, the MOM is interposed between cytosol and IMS, causing transport impediment which is not negligible (41). On the basis of the membrane permeability coefficients for ADP and ATP used in the model of Vendelin et al. (41), the conductance of MOM, PS_{mom}, is calculated to be 0.10 s^{-1} for ADP and ATP; see APPENDIX B. Given the high diffusivity in the cytosol, the total conductance PS_{tot} between myofibril and intermembrane space with diffusion in the cytosol and permeation of the MOM in series is therefore virtually the same as PS_{mom}. For PCr and Cr, the outer membrane conductance PS_{mom} = 162.5 s^{-1} and total conductance PS_{tot} = 155 s^{-1}; for P_i PS_{mom} = 204 s^{-1} and PS_{tot} = 194 s^{-1} (APPENDIX B, parameter set II).

Beard (28) used the same membrane permeabilities, except for ADP and ATP where a higher permeability was estimated based on measurements on isolated mitochondria. This results in PS_{mom} = 53.1 s^{-1} and PS_{tot} = 51.9 s^{-1} for ADP and ATP (APPENDIX B, parameter set III).

Saks et al. (32) reported in a later experimental study on permeabilized fibers that diffusibility in the cytosol was 6% of the previously assumed diffusibility (41), and membrane permeability *P* was 3% of previous reference values 260 μm/s for PCr and Cr, 327 μm/s for P_i, and 145 μm/s for ADP and ATP. These values were thought to explain the experimentally determined ADP affinity of the mitochondria in permeabilized fibers (32). This results in parameter set IV which is also tested in the present model: $PS_{tot,ATP} = PS_{tot,ADP}$ = 2.6 s^{-1}, $PS_{tot,PCr} = PS_{tot,Cr}$ = 4.6 s^{-1}, and $PS_{tot,Pi}$ = 5.8 s^{-1}.

Parameter set V is the same as parameter sets II and III, with the exception of the PS_{tot} for ADP and ATP, which is optimized to yield the experimentally determined t_{mito}, 3.7 s. APPENDIX B gives details on the parameter sets and their calculations.

Model calculations. The model was implemented in "R" (37), which is an object-oriented high-level computer language and analysis environment often used for scientific computing, in particular for statistical analysis of microarray data (http://www.r-project.org). R was also applied to simulation of ecological models (31). The R language supports flexible data structures, and is open source, allowing extensions and modifications by the user. R is free of charge with a large user community that supplies a vast library of analysis routines. Model simulations were run on 1.5–3 GHz desktop personal computers and a 1.7-GHz Pentium laptop computer with 512–1,024 kB RAM on a Windows XP platform.

The ordinary differential equations in the model are integrated using the Livermore solver developed by Petzold et al. (30), which switches algorithms automatically during execution to handle stiff and non-stiff conditions. As an additional check to assess whether the equations were correctly integrated the concentrations of conserved moieties (*Eqs. 18–20* in APPENDIX A) were calculated and found to change by <10 μM during the simulation of a response, demonstrating good numerical accuracy.

Optimized parameter values were obtained using the R-routine "optim," based on the "L-BFGS-B" algorithm (8), which allows box constraints on the parameters which are optimized. For optimization of a single parameter a golden section search and successive parabolic interpolation, implemented in the R routine "optimize" was used. Computation times for optimization with the pulsatile forcing function were an order of magnitude larger than when ATP hydrolysis was constant over the cardiac cycle. Parameter optimization was therefore done with the latter approach. Response results are very similar, with t_{mito} usually 0.1–0.2 s larger for the pulsatile than the continuous forcing function.

Experimental data on dynamic response of oxidative phosphorylation. The dynamic response of oxidative phosphorylation has been determined under a great number of experimental conditions for heart muscle. The time course of the increase of O_2 uptake in the mitochondria in response to step changes in cardiac pacing rate was determined. These changes in workload resulted in immediate

changes in ATP hydrolysis in the myofibrils and at ion pumps, reflected by systolic peaks of initial heat generation (45). However, OxPhos is reflected by slow recovery heat generation and responds with clearly measurable delay to changes in ATP hydrolysis. An increase of O_2 consumption in the muscle cells results in an increase in O_2 uptake from the perfusate flowing through the capillaries, which after a delay caused by intravascular convective transport results in a decrease in cardiac venous O_2 concentration, measurable with O_2 electrodes in isolated hearts. The time course of O_2 uptake measured at the level of the whole heart was corrected for the O_2 transport delay between the mitochondrial site of O_2 consumption and the cardiac venous O_2 electrode. This deconvolution can be accurately done for the average response time (40), but the full time course of O_2 consumption following a heart rate step cannot be accurately reconstructed. The definition of the response time t_{mito} to a step function increase in cardiac pacing is

$$t_{mito} = \int_0^\infty \{[V_{O_2}(t) - V_{O_{2end}}]/[V_{O_2}(0) - V_{O_{2end}}]\} \cdot dt \qquad (3)$$

where $V_{O_2}(t)$ is the time-dependent oxygen consumption at the level of the mitochondria and $V_{O_{2end}}$ is the final oxygen consumption reached asymptotically if the changed pace rate is sustained. The denominator gives the amplitude of the response of O_2 consumption to the step in pace rate, with $V_{O_2}(0)$ the oxygen consumption in the steady state before the challenge is applied. If the O_2 consumption decreases exponentially after a downward step in pacing rate, t_{mito} is equivalent to the time constant of the exponential function. In systems theory terms, the definition in *Eq. 3* is equivalent to the first statistical moment of the impulse response function. Because t_{mito} was corrected for delays due to O_2 transport in the blood vessels and by diffusion, t_{mito} reflects the dynamic response at the level of the mitochondria. The method to obtain it during studies on isolated hearts has been validated in several studies, as reviewed in Ref. 39. The experimental values for t_{mito} are compared with model results in the present study.

In experiments the integral of *Eq. 3* is taken for a limited period of time, ~1 min, because drift of the O_2 electrode and the biological preparation preclude longer measurements. For direct comparison with the experimentally measured t_{mito}, t_{mito}-exp is calculated from the simulations by replacing $V_{O_{2end}}$ in numerator and denominator of *Eq. 3* with V_{O_2} calculated at 60 s in the simulation and integrating over 60 s. The true t_{mito} value was calculated from the simulations by integrating until the steady state had been virtually fully reached. Simulations demonstrate that t_{mito}-exp may underestimate the true t_{mito} in some cases. If the response is close to an exponential response, *Eq. 3* integrated over 60 s gives adequate results. However, the simulations showed that for low CK activities, the response of ATP synthesis is initially very quick but shows a tail, which deviates for a long time from the asymptotic end value.

RESULTS

Dynamic response of mitochondrial ATP synthesis to a step in heart rate. Figure 2 shows the model simulation of an experiment, in which the paced heart rate was increased from 135 to 220 beats/min in isolated rabbit hearts (17). A change in myocardial O_2 consumption from 22.0 to 28.4 μmol·g dry mass^{-1}·min^{-1} was measured in the experiment, corresponding with an estimated ATP hydrolysis increase from 487 to 628 μmol/l cell water/s. These values are averaged over the cardiac cycle. The forcing function of ATP hydrolysis shown in Fig. 2 represents the pulsatile nature of ATP consumption during the cardiac cycle (41, 45). The peak value is six times the average value. Note that the amplitude of ATP hydrolysis is reduced ~23 times at the level of ATP synthesis, demonstrating the damping characteristics of the system. A substantial pulsatile component remains, with amplitude about one-fourth of the average ATP synthesis. Despite the clearly pulsatile response of ATP synthesis to each systolic pulse of ATP hydrolysis, the response to a step in heart rate has a slow component with a response time ("time constant") equivalent to ~14 cardiac cycles. ATP production averaged over the cardiac cycle equals average ATP hydrolysis in the steady state before the change in heart rate at $t = 0$. Cardiac cycle-averaged ATP synthesis approaches the increased average ATP hydrolysis again at the end of the response shown in Fig. 2.

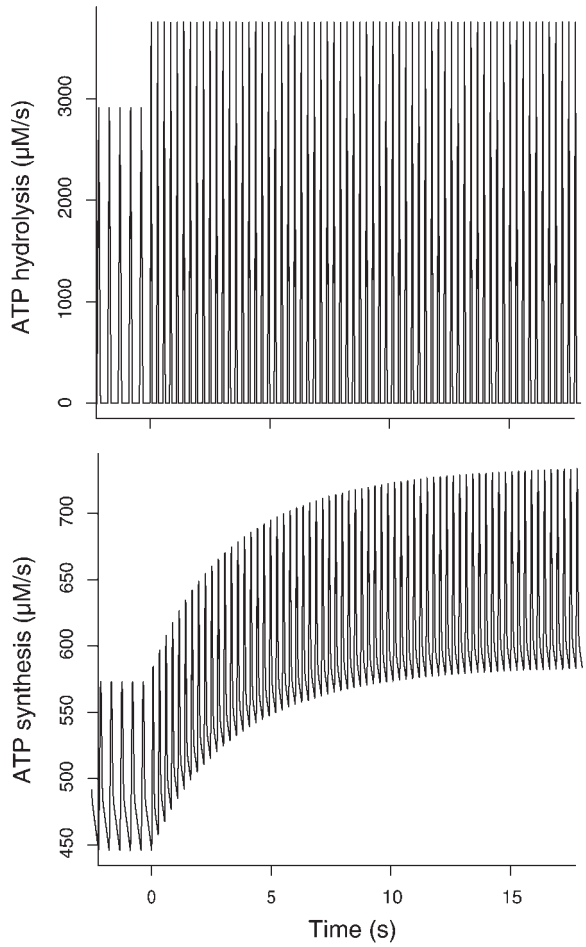

Fig. 2. Time course of ATP production by the mitochondria in response to a step in heart rate from 135 to 220 beats/min, resulting in a step in ATP hydrolysis from 486.5 to 627.6 μmol·l cell water^{-1}·s^{-1} (values averaged over the cardiac cycle). Note the difference in scale between ATP hydrolysis and ATP synthesis, and note further that the peak value of ATP hydrolysis is sixfold higher than the time average. *Top*, the pulsatile forcing function, which represents ATP hydrolysis during cardiac systole. *Bottom*, the response of mitochondrial ATP production. The system damps the pulsations in ATP hydrolysis resulting in ~23-fold reduction in amplitude at the level of ATP synthesis. The total cytosolic diffusion and membrane permeation conductances for ADP and ATP are $PS_{tot,ADP} = PS_{tot,ATP} = 13.3$ s^{-1}, resulting from optimization to reproduce the experimentally measured response time.

In the experiment glycolysis was completely blocked and pyruvate given as substrate to bypass glycolysis, corresponding with the absence of glycolytic ATP production in the model, yielding a measured response time t_{mito} (see *Eq. 3*) of 3.7 s (17). In the simulation of Fig. 2, an optimized value for the transport conductance, $PS_{tot,ADP}$, and $PS_{tot,ATP}$, of 13.3 s^{-1} was

used, yielding a t_{mito} of 3.7 s, in correspondence with the experimental result. This is parameter set V (see APPENDIX B). Details of the optimization and results for other values for $PS_{tot,ADP}$ and $PS_{tot,ATP}$ are discussed below.

Test of restricted diffusion across MOM. The effect of different sets of diffusion and membrane permeation parameters on the response time to a heart rate step is conveniently demonstrated in a graph based on the rectangular, rather than pulsatile, forcing function for ATP hydrolysis (Fig. 3). The response time for the pulsatile forcing function, calculated according to *Eq. 3*, is 0.1–0.2 s larger than the result for a continuous forcing function which is constant during the cardiac cycle. The dynamic response to a sudden change in cytosolic ATP hydrolysis was simulated (Fig. 3) with the five sets of membrane permeability parameters given in APPENDIX B, keeping the other model parameters constant.

The diffusion coefficients used to calculate model parameters for the simulation were taken from NMR diffusion measurements (11). If any further restriction in MOM permeation was neglected for all metabolites in the model (parameter set I), the response of ATP production was roughly exponential with t_{mito} = 2.4 s. This is slightly faster than found in the experiments, where the time constant is 3.7 ± 0.3 s (means ± SE) if glycolysis is inhibited and bypassed (17). The difference between simulation and experiment is >4 times SE, suggesting that the assumption of very high membrane permeability is incorrect.

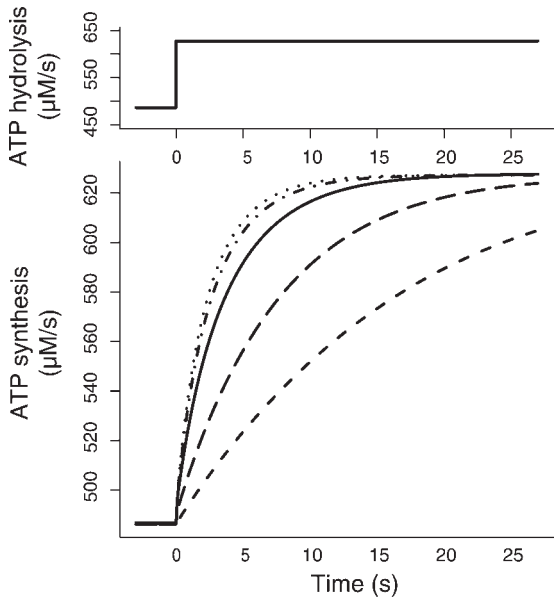

Fig. 3. Time course of ATP production by the mitochondria (ATP synthesis) in response to a step in ATP hydrolysis from 486.5 to 627.6 μmol·l cell $water^{-1}\cdot s^{-1}$ (values averaged over the cardiac cycle) for five different sets of diffusion and membrane permeation parameters PS. *Top*, for clarity, the nonpulsatile forcing function for ATP hydrolysis was used. The response times (*Eq. 3*) differ 0.1–0.2 s between the nonpulsatile and pulsatile forcing functions. The five sets of permeability parameters given in APPENDIX B result in the following: the dotted curve for diffusivity parameters in the cytosol corresponding with NMR diffusion measurements with negligible permeation restriction of the outer mitochondrial membrane, with "time constant" t_{mito} = 2.4 s (parameter set I, see APPENDIX B); the short-dashed curve takes severe permeability restrictions of the outer membrane for ADP and ATP into account in addition to cytosolic diffusion, using the membrane permeation parameters for PCr, Cr, ADP, ATP, and P_i of Vendelin et al. (41), with t_{mito} = 14.8 s (parameter set II); the dash-dotted curve, with t_{mito} = 2.7 s, uses the same parameters as in parameter set II, except that the higher membrane permeability parameters for ADP and ATP of Beard (4) are used (parameter set III); the long-dashed curve is for the membrane permeation parameters found in the model analysis of Saks et al. (32) with cytosolic diffusivity reduced to 6% and membrane permeability reduced to 3% of reference values, with t_{mito} = 7.25 s (parameter set IV); the continuous line is the result an optimization procedure in which the diffusion conductance parameter for ADP and ATP is optimized to $PS_{tot,ADP} = PS_{tot,ATP} = 13.3\ s^{-1}$ to yield the experimentally determined value of t_{mito} = 3.7 s (parameter set V); the other parameters are the same as in sets II and III.

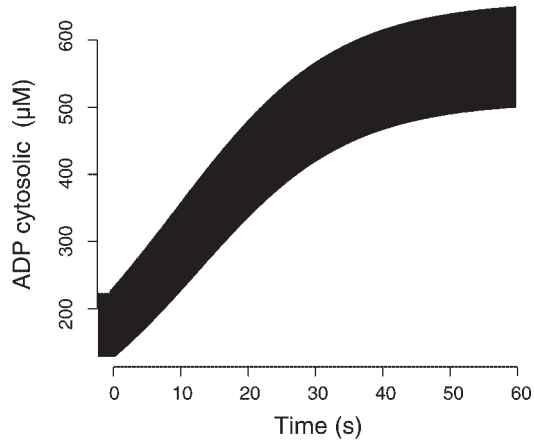

Fig. 4. Predicted response of the cytosolic ADP concentration to step in pulsatile ATP hydrolysis at $t = 0$ (see Fig. 2), simulated with parameter set II (APPENDIX B) reflecting restricted permeation of ADP and ATP across the MOM (see Fig. 1). $PS_{tot,ADP} = PS_{tot,ATP} = 0.1\ s^{-1}$ calculated from permeation parameters in Ref. 41. The response is much slower and ADP concentrations are much higher than measured experimentally (13).

A restriction in MOM permeation for ADP and ATP was added to the model, using membrane permeation parameter 0.16 μm/s for ADP and ATP as assumed in Vendelin et al. (41). This means that ADP and ATP transport is strongly restricted, simulating a condition in which a "phosphocreatine shuttle" operates (parameter set II, APPENDIX B). MOM permeabilities for Cr, PCr, and P_i corresponded with those in published mathematical models (4, 41) and are much higher than for ADP and ATP. The simulated response for this parameter set was characterized by t_{mito} = 14.8 s (see Fig. 3), much slower than the experimental value of 3.7 s. Using the pulsatile forcing function (see Fig. 2), the cytosolic ADP concentration increased from a value oscillating from 134–217 μM to 500–650 μM (Fig. 4) for this low MOM permeability, which is much higher than derived from end-diastolic NMR measurements in this experimental model (13). The end-diastolic PCr concentration decreased from ~3,230 to ~990 μM, which is much lower than measured experimentally (13). End-diastolic P_i values changed from ~3,470 to ~6,060 μM, much higher than the experimental findings (13). A 20% reduction in CK activity led to a doubling of ADP concentration for these MOM permeabilities. It is clear that the results of the dynamic simulation with this parameter set with very low ATP and ADP permeability, reflecting a "phosphocreatine shuttle" condition, deviate substantially from experimental values.

The set of diffusion and permeability parameters (32) with less restricted ADP and ATP membrane permeability, $P_{mom,ATP} = P_{mom,ADP}$ = 4.35 μm/s, and with diffusibility in the cytosolic space ~6% of previous values (41), yielded t_{mito} = 7.25 s, which is still >10 times means ± SE removed from the experimental value (parameter set IV, APPENDIX B).

The membrane permeation parameter 85 μm/s for ADP and ATP from the model of Beard (4), based on measurements of Lee et al. (28), resulted in $t_{mito} = 2.7$ s, which is ~3 times the SE removed from the experimental value (parameter set III, APPENDIX B).

The MOM conductance for ADP and ATP is of major importance for theories about the phosphocreatine shuttle and regulation of mitochondrial ATP synthesis, but is apparently not well known, as demonstrated by the considerable differences in its value between various models and experimental results (4, 24, 25, 32, 41). The other parameters in the present model were either measured independently in the same experimental model in the same laboratory (CK activities, mitochondrial aerobic capacity, metabolite concentrations), or represent well established literature values for kinetic constants of enzyme processes (MM-CK, Mi-CK, oxidative phosphorylation). The permeability parameters for PCr, Cr, and P_i (PS_{PCr}, PS_{Cr}, PS_{Pi}) were used in various models with some degree of consensus. The diffusivity and permeability for ADP and ATP are not well known and were therefore estimated from the dynamic response experiment (Fig. 3). $PS_{tot,ADP}$ and $PS_{tot,ATP}$ were set equal to each other and optimized with a golden section search to reproduce the experimental value of $t_{mito} = 3.7$ s, which resulted in $PS_{tot,ADP} = PS_{tot,ATP} = 13.3\ s^{-1}$ (parameter set V, APPENDIX B). This permeability value, "reverse engineered" from the experimental response, is ~130-fold higher than the PS value derived from the permeability in the model of Vendelin et al. (41) with severe ADP and ATP permeability restriction, about 4-fold higher than the ATP and ADP conductances resulting from the analysis of permeabilized fiber experiments by Saks et al. (32) and about 4-fold lower than the value based on the model of Beard (4).

Effects of changes in CK activity on dynamic response of oxidative phosphorylation. The two CK isoforms are key molecules in the "skeleton model." Therefore the dynamic response of OxPhos to the heart rate step was calculated as function of the CK activity, to simulate partial inhibition or overexpression of CK in the model. Figure 5 shows how t_{mito} varies with the relative CK activity (V_{CK}) when the mitochondrial and the cytosolic activity of CK were changed in parallel by the same factor. For relative CK activity $V_{CK} = 1$, the CK activities are equal to those measured in rabbit hearts in the experimental group, resulting in $t_{mito} = 3.7$ s. For $V_{CK} > 0.03$ the response becomes faster if V_{CK} increases. However, if V_{CK} falls below 0.03, t_{mito} drops steeply (Fig. 5*A*, continuous line). This applies to the true t_{mito}, calculated according to *Eq. 3* for a period of time sufficient to reach the new steady state. However, t_{mito}-exp, calculated for a 1-min recording period as done experimentally (see *Experimental data*), is already affected at higher V_{CK} values (Fig. 5*A*, dotted line). Figure 5*B* gives t_{mito} also for high V_{CK} where t_{mito} decreases further.

The true t_{mito} and t_{mito}-exp value calculated for a 1-min recording as in the experiments differ at low V_{CK} because it takes ATP synthesis very long to approach the steady-state value. In Fig. 6, the predicted response of ATP synthesis to a heart rate step is shown for V_{CK} at 1.5% of the reference value. The model predicts an immediate steep increase in ATP synthesis, followed by a slow, gradual increase, which forms the major contribution to the t_{mito} value calculated from *Eq. 3*. However, the slow change in the experiments, which still occurs after 60 s, cannot be reliably measured because of drift and fluctuations in the physiological system and measurement equipment. Therefore the steady-state value was measured at ~1 min in the experiments. The model analysis makes this weakness in the experimental design clear. The dotted lines in Fig. 5, *A* and *B*, give an approximation of t_{mito} as actually calculated from the experimental measurement (see METHODS).

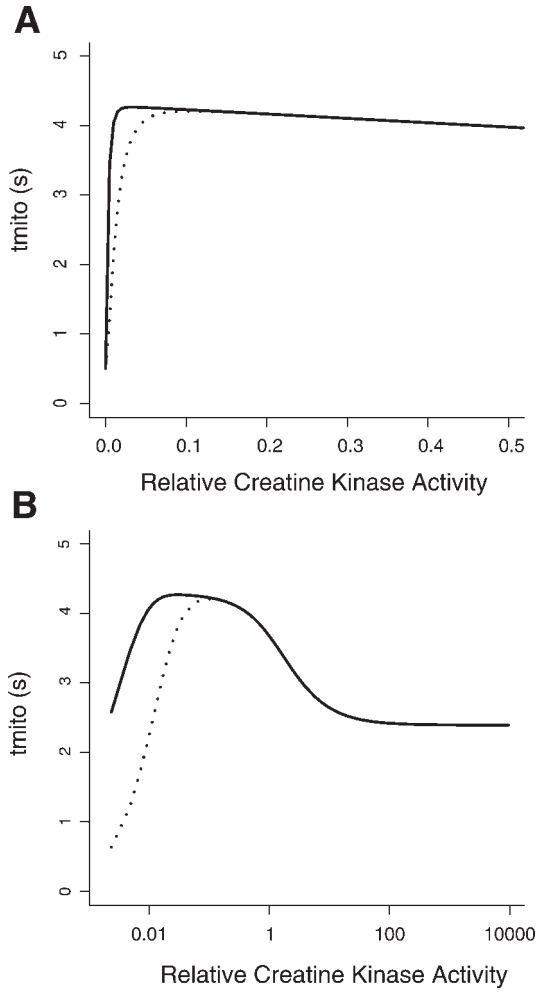

Fig. 5. The response time of mitochondrial ATP production, t_{mito}, to a step in heart rate and therefore ATP hydrolysis as function of the relative CK activity. The t_{mito} is predicted for a step in heart rate from 135 to 220 beats/min, leading to an increase in ATP hydrolysis from 486.5 to 627.6 μmol·l cell water^{-1}·s^{-1} (value averaged over the cardiac cycle). Relative CK activity, V_{CK}, is given as a fraction of the value measured in normal rabbit hearts (17, 18). The Mi-CK and MM-CK activities change in parallel. *A*: linear plot for low V_{CK}. The continuous line is the true t_{mito} measured if the response that can be followed is sufficiently long. The dotted line represents t_{mito}-exp that is calculated if the response for oxidative phosphorylation is measured for 1 min as in the experiments. For low V_{CK}, the full response amplitude has not yet been reached at that time. *B*: true t_{mito} (continuous line) and the t_{mito}-exp determined from a 1-min curve (dotted line) as function of V_{CK}, plotted logarithmically, for the same conditions as in *A*.

For $V_{CK} < 0.1$ the experimental version of t_{mito} decreases with decreasing V_{CK}. In the experiments (17), t_{mito} at $V_{CK} = 0.023$ was measured to be 2.6 s, significantly lower than the 3.7 s at $V_{CK} = 1$, in agreement with the prediction of the model calculation (Fig. 5, dotted line).

To determine the contributions of each of the two isoforms, in Fig. 7, t_{mito} is given as function of the activities of Mi-CK and MM-CK, varied independently of each other. If MM-CK

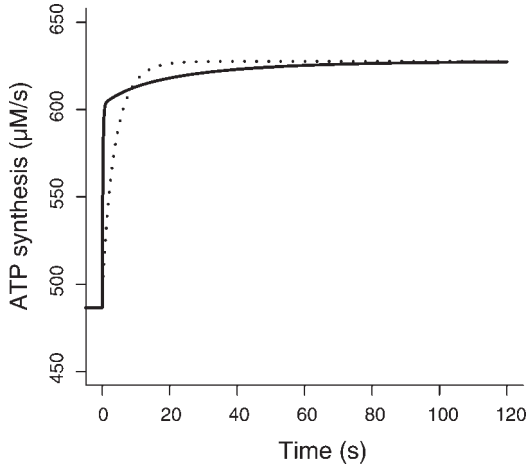

Fig. 6. The time course of mitochondrial ATP synthesis, averaged over the cardiac cycle, in response to a step in heart rate from 135 to 220 beats/min. ATP hydrolysis is increased from 486.5 to 627.6 μmol·l cell water^{-1}·s^{-1} (averaged over cardiac cycle). The dotted line gives the response for relative CK activity 1. The continuous line gives the response for CK activity at 1.5% of the normal value (V_{CK} = 0.015). In the latter case, there is an almost immediate jump in ATP synthesis, followed by a very slow approach to the final value, and the t_{mito}-exp value calculated for the first 60 s is substantially smaller than the true t_{mito}. Although the initial response is slower for V_{CK} = 1, within 10 s, ATP synthesis is higher than for V_{CK} = 0.015. The t_{mito}-exp calculated for a 60-s recording is therefore almost equal to the true t_{mito} for V_{CK} = 1, but substantially lower for V_{CK} = 0.015.

activity is kept constant at its reference level V_{CK} = 1, an increase in Mi-CK activity always leads to a decrease in t_{mito}. If Mi-CK activity is kept constant at V_{CK} = 1, increases in MM-CK activity always lead to increases in t_{mito}. The decrease of t_{mito} above V_{CK} = 0.03 in Fig. 5 apparently is caused by the increase in mitochondrial CK activity. Increasing relative Mi-CK activity from 0 to 3 at constant $V_{MM\text{-}CK}$ = 1 causes t_{mito} to decrease from 4.5 to 3.0 s, demonstrating the accelerating effect of phosphocreatine transport into the IMS on the dynamic adaptation of OxPhos to ATP hydrolysis. If the MM-CK activity reaches zero, this results in t_{mito} = 2.4 s. The remaining Mi-CK activity is then still 7.7% of the normal MM-CK activity. If the Mi-CK activity is subsequently also completely abolished, t_{mito} becomes 0.5 s.

Predicted metabolite patterns as function of CK activity. Metabolite concentrations in the steady state at the two levels of ATP hydrolysis, 135 and 220 beats/min, are shown in Fig. 8 as a function of relative CK activity. In Fig. 8, *A* and *B*, results for the rabbit heart parameters are given. PCr concentration decreases ~10% with increasing ATP hydrolysis, in agreement with NMR measurements in rabbits at two heart rates (13). This decrease depends very little on CK activity, except at very low V_{CK} values. ADP in the intermembrane space increases slightly with ATP hydrolysis, 39 to 43 μM for the heart rate step at V_{CK} = 1. In the cytosol ADP increases from 64 to 77 μM. The major part of the increase in ATP synthesis is caused by the increase of P_i concentration in the IMS from 910 to 1,552 μM. These values are only ~3 μM lower than in the cytosol. The P_i increase with heart rate mirrors the decrease in PCr concentration.

Dependence of metabolite levels and dynamic response on metabolic system parameters. The dependence of metabolite levels and t_{mito} on relative CK activity is not very strong, at least for $V_{CK} > 0.1$. However, this effect can be much larger for other parameter sets. To demonstrate this, results are given in Fig. 8, *C* and *D*, for parameters applicable to the rat heart. These parameters, given in Table 2, were compiled in Ref. 23, among others from data in Refs. 2 and 44. The CK activity, mitochondrial aerobic capacity and metabolite levels are higher than those applicable to Fig. 8, *A* and *B*. As a result, the PCr concentration is higher and ADP in the IMS is lower than in the simulations for rabbit heart. $PS_{tot,ADP} = PS_{tot,ATP} = 13.3\ s^{-1}$ is also used for the rat heart simulations. For the rat parameters the cytosolic ADP concentration increases from 17.1 to 20.7 μM at V_{CK} = 1 during the heart rate step, while the IMS ADP concentration changes from 6.68 to 6.78 μM. The ADP in the IMS now depends strongly on relative CK activity and hardly changes with heart rate for V_{CK} in the range 1–2. The increase in ATP synthesis in this range is completely caused by changes in P_i, which increases virtually as much as PCr decreases. Both metabolite levels (Fig. 8) and t_{mito} (Fig. 9) depend much more strongly on relative CK activity in rat heart than in rabbit heart. The t_{mito} reaches 8 s at low CK activities. Note that the decrease in PCr for the step in ATP hydrolysis is low for high relative CK activity in Fig. 8*C*. This is close to experimental results which often show no significant changes in PCr with cardiac workload (19). Note that calcium stimulation of the mitochondria at longer time scales, not included in the model, may reduce changes in PCr in the steady state further.

Contribution of PCr to phosphoryl group transport from the mitochondria. For the standard rabbit parameter set, at ATP hydrolysis rate 486.5 μM/s the diffusion flux carried by PCr is 154 μM/s and by ATP is 333 μM/s. If the activity of both CK isoforms is increased 3-fold this becomes 281 and 206 μM/s. If Mi-CK only is threefold increased in activity this becomes 256 and 230 μM/s.

For the rat heart parameter set, with higher Mi-CK and MM-CK activities than for rabbit, the flux carried by PCr is 349 and by ATP 138 μM/s. This becomes 430 μM/s for PCr

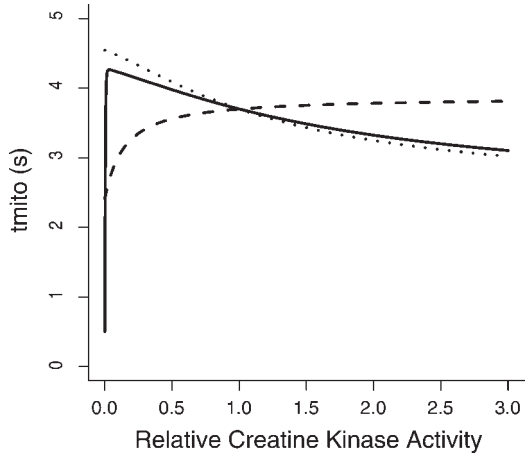

Fig. 7. The true response time of mitochondrial ATP synthesis, t_{mito}, to a step in heart rate and ATP hydrolysis as function of the relative CK activity for the rabbit parameter set (see Table 2). The continous line gives t_{mito} with Mi-CK and MM-CK activities both changed by the same factor, as in Fig. 5. The dotted line gives the t_{mito} changes if the Mi-CK activity is changed with relative MM-CK activity kept constant at its normal value, V_{CK} = 1. The dashed line gives the t_{mito} changes if the MM-CK activity is changed and the relative Mi-CK activity is kept constant at its normal value, V_{CK} = 1, with t_{mito} reaching 2.41 s at relative MM-CK activity zero.

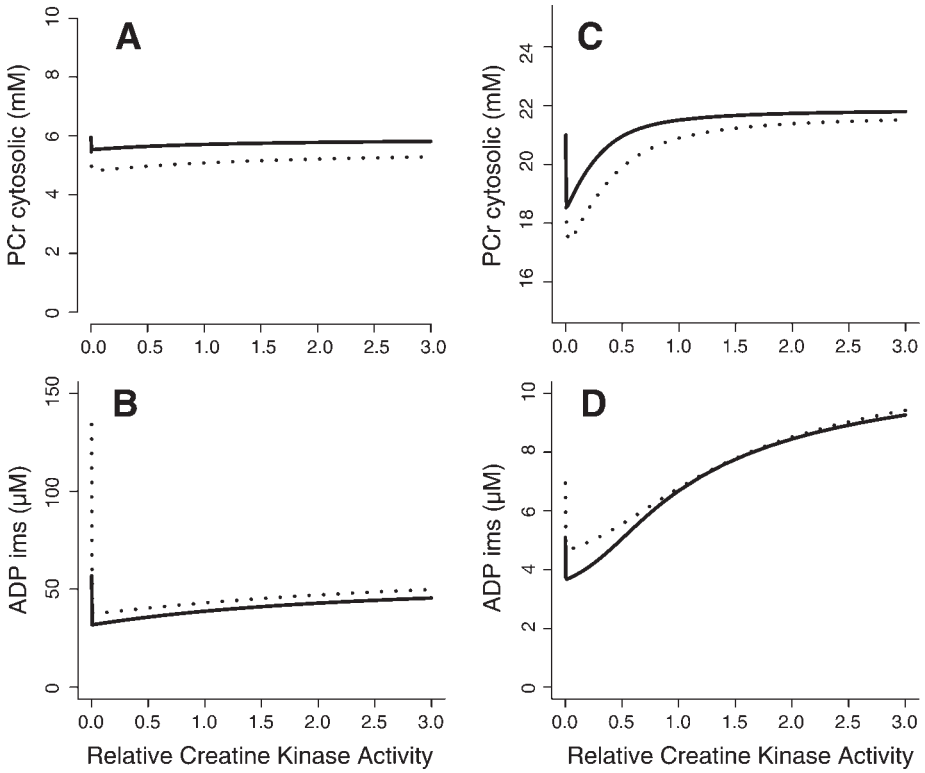

Fig. 8. *A* and *B*: standard parameters in the rabbit heart experiment (see Table 2). *C* and *D*: different set of parameters for rat heart (see Table 2). Note the differences in scale. Steady-state metabolite levels as a function of relative CK activity at two levels of mitochondrial ATP hydrolysis: 486.5 (continuous line) or 627.6 (dotted line) μmol/l cell water/s, resulting from heart rates 135 and 220 beats/min, respectively. MM-CK and Mi-CK are changed in parallel. Values were constant over the cardiac cycle in this simulation. Results for phosphocreatine concentrations in the cytosol and ADP in the intermembrane space (ims) are given.

and 57 μM/s for ATP if CK activities are three times higher than the normal rat values.

Predictions for metabolite oscillations as function of MM-CK and Mi-CK activities. The model predicts that ADP levels and ATP production oscillate appreciably (see Fig. 10) because of the pulsatile hydrolysis of ATP. For P_i, the average level is increased at low V_{CK}, with little change in the amplitude of pulsation, which is 141–146 μM for V_{CK} 0–3. This lack of change in P_i oscillation reflects that CK does not buffer P_i directly. When CK activity is increased above its normal level the oscillations become less strong, and the average P_i concentration drops further. For low CK activity, at a similar level as in the experiment with CK inhibition (17), the predicted oscillation of ATP synthesis and of cytosolic ADP concentration becomes very strong.

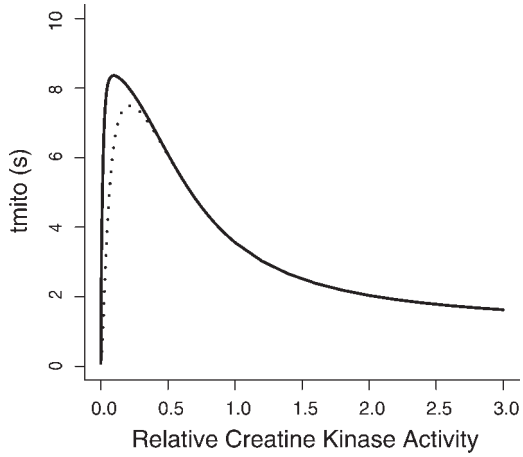

Fig. 9. The response time of mitochondrial ATP production, t_{mito}, to a step in heart rate causing a step in ATP hydrolysis, as function of the relative CK activity for the rat heart parameter set (see Table 2). The changes in CK activity are applied in parallel to MM-CK and Mi-CK and are given relative to the reference values for the rat heart parameter set. The relative changes in t_{mito} are considerably larger than in Fig. 5, and the top of the curve is shifted to a higher V_{CK}. The continuous line gives the true t_{mito}; the dotted line gives the t_{mito}-exp as calculated during experiments where the response is followed for 1 min.

DISCUSSION

The modular approach to developing models of biomolecular systems. In this study, we try to understand the first phase of regulation of oxidative phosphorylation in adaptation to quickly changing ATP hydrolysis in the cardiomyocyte. One of the difficulties in modeling this process is that it takes place in an environment containing thousands of molecular species in a densely connected molecular network. Our approach is to develop a "skeleton model" containing only a few key processes, hypothesized to explain the fast regulation of oxidative phosphorylation. If shown to function correctly, this "skeleton model" can be treated as a module in a comprehensive model for the cellular metabolic system. This ACP module could then be linked to a detailed module for oxidative phosphorylation. Another module could describe ATP hydrolysis in the myofibrils, regulated by calcium ions and containing feedback regulatory effects of ADP and P_i on the ATP hydrolysis process and on force and speed of muscle contraction.

Given that the complete system contains thousands of molecular species and that these molecules tend to be very densely connected in extensive networks, it is not a priori clear to what extent a modular approach is possible (38). However, although the structure of the system in terms of possible molecular interactions shows very high connectivity that makes it difficult

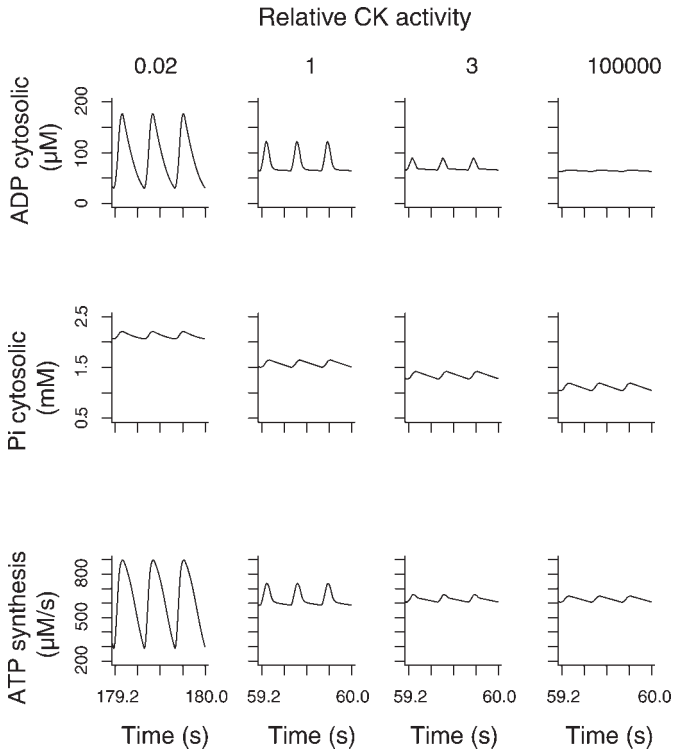

Fig. 10. Oscillations of ADP and P_i concentrations in the cytosol, and ATP production by the mitochondria caused by pulsatile ATP hydrolysis as in Fig. 2, shown for various relative CK activities. Simulation results are given in the steady state, 180 s (for $V_{CK} = 0.02$) or 60 s (higher V_{CK}) after changing heart rate from 135 to 220 beats/min and ATP hydrolysis to 627.6 μM/s. MM-CK and Mi-CK activities are changed in parallel. The standard rabbit parameter set from Table 2 was used for the simulation.

to discern modules at the structural level, it may be feasible to discern modules at the kinetic level (D. A. Fell, unpublished communication). The module investigated here was tested under conditions of blocked glycolysis and exclusively for the first phase of the dynamic response of OxPhos to isolate it experimentally as much as possible from the complete biomolecular system.

The tests performed in this paper suggest that the ACP module may be sufficient to explain the first phase of fast regulation of OxPhos. Predictions were made for further testing of the model. In the module, use was made of kinetic parameters, which had been determined independently by measurements on isolated components of the system. However, the permeability of the MOM to ADP and ATP was optimized from measurements on the behavior of the system as a whole because there was no consensus in the literature on this parameter. Thus a constraint based on a higher-level function was used in conjunction with knowledge on the molecular constituents of the model. It is possible to improve the description of the modules which communicate with the ACP module, and retest the integrated model in an iterative cycle. Although further experimental testing with new experimental data and with improved ATP production and cytosolic ATP hydrolysis models is desirable, these first results suggest that the present model of the ACP module is sufficient to explain the first phase of the dynamic adaptation of OxPhos to ATP hydrolysis in cardiomyocytes.

The alternative to working with a modular "skeleton model" is to start directly with large models containing a large number of molecular processes. Many of the details in such a model will probably be wrong to a smaller or larger extent. Furthermore, models with all molecular details are hard to understand and debug. A small model containing only the key processes determining the overall process is preferable to understand the essential characteristics of the process. A beautiful example of a "skeleton model" approach is a model for an ecological system (6) with just three variables (vegetation, consumers, and predators), explaining the chaotic variation in the amplitude of peaks in the populations of hares and lynxes while the periodicity of the peaks is regular and peaks are synchronized between neighboring populations. Weaker interactions with many other species were ignored and nevertheless the essential behavior of the ecological system was retrieved.

Topdown experimental systems biology usually means fishing for relations amongst a large number of high density molecular measurements obtained for a limited number of experimental conditions. This usually does not lead to immediate improvement of mechanistic models of the system (20, 38), among others because testing of many relationships in such data sets leads to high false positive rates. Such an inductive approach of purely data-driven discovery of facts cannot replace the scientific cycle of testing and improving mechanistic models of the system (38). Large scale models (e-cells, silicon cells) that contain all mechanisms of interactions are not yet feasible because kinetic parameters and descriptive equations for many of the interactions are lacking. Designing and testing models for modules that may be assembled in larger models in subsequent steps may be a feasible strategy to build models of the whole system.

Regulation of oxidative phosphorylation via ADP and P_i. It has been debated whether mitochondrial ATP production in cardiac muscle is regulated via concentration changes in ADP and P_i, or that additional mechanisms play a role (19). Ca^{2+} entry into the mitochondria, where it stimulates matrix dehydrogenases and may regulate other sites in oxidative phosphorylation may play an important regulatory role (7, 10), although at longer time scales (time constant 20–25 s) than considered here (~4 s). An additional calcium signaling module would be needed to simulate this slow regulation. Even slower regulatory changes are conceivably involved, such as changes in synthesis and breakdown of the mitochondria. However, the present study is limited to the fast phase only.

The ACP module may be sufficient to explain the first phase of stimulation of oxidative phosphorylation, as shown in the present study. However, the membrane permeation parameter for ADP and ATP transport across the MOM was unknown and had to be estimated from the overall response of the system. To corroborate this finding, independent studies on MOM permeability are desirable. The model may be further tested based on its predictions, for instance on the oscillation of cytosolic metabolites and metabolite levels for different CK activities (Fig. 10) due to overexpression or inhibition of the mitochondrial and cytosolic isoforms of CK. For the moment, the hypothesis that the ACP module can explain the fast response of oxidative phosphorylation appears plausible. Note in particular that the model indicated that processes in the mitochondrial matrix play a negligible role in the delay of ATP produc-

tion in response to changing ATP hydrolysis, as detailed in METHODS.

The glycolytic chain seems to play an important role in the dynamic response, increasing the response time from ~4 with blocked glycolysis to ~8 s if glycolysis is active (17). A remarkable finding by NMR spectroscopy during heart rate steps is that P_i, PCr, and by inference ADP, change with a time constant of roughly 2.5 ± 2 s, while in the same study t_{mito} was 11 s. In these experiments, showing the delayed response of OxPhos with respect to the changes of the phosphate metabolites located mainly in the cytosol (13), glycolysis was fully functional. Note that the isolation procedure of the hearts in these experiments entailed a period of ischemia, which may increase t_{mito} (46). Based on the simultaneous NMR and t_{mito} data, we hypothesized that glycolysis is able to delay changes of ADP and P_i in the mitochondrial intermembrane space relative to the myofibrillar core. Increased glycolytic capacity after a brief period of ischemia may then further delay the dynamic response of OxPhos (46). Thus the ACP module probably shows a strong interaction with glycolysis, a complexity which was experimentally removed from the present study by blocking glycolysis and giving a substrate for the TCA cycle which bypasses glycolysis.

With the estimated permeability parameter $PS_{ATP} = PS_{ADP} = 13.3\ s^{-1}$ the concentration difference across the outer mitochondrial membrane is 56 μM at half of the maximum ATP synthesis rate of the mitochondria. Adding this to the K_M for mitochondrial ATP production for ADP in the intermembrane space the apparent K_{ADP} for intact mitochondria is predicted to be ~80 μM. This is higher than the maximum K_{ADP} value estimated for mitochondria in skinned cardiac muscle fiber experiments (25) and compatible with the suggestion that isolation of mitochondria (32) or perhaps even skinning of muscle fibers leads to a decrease of diffusional restriction for ADP across the MOM, which is present in the mitochondria in situ.

Although other regulatory factors, such as Ca^{2+}, very likely play a role at longer time scales (7, 10), the fast adaptation of OxPhos to cytosolic demand is explained by regulation via changes in ADP and P_i in the intermembrane space. The lack of appreciable changes in PCr value at increased cardiac workload was often regarded as a sign that ADP and P_i are not the prime regulators of OxPhos. Figure 8 demonstrates that the decline of PCr depends on the parameter values and can be small for some parameter sets, even under the assumption that only ADP and P_i regulate OxPhos. ADP changes in the intermembrane space can be almost absent and P_i is then the main regulator of OxPhos for some parameter combinations. Stimulation of mitochondrial ATP synthesis via calcium ions is not included in the simulations for Fig. 8 and leads to even smaller changes in PCr. Figure 8 demonstrates that altered conditions of the system, for instance caused by altered levels of gene expression, can lead to a rather broad range of system behavior.

Role of CK in cardiac muscle cell. CK has been proposed to play several roles in muscle energy metabolism. CK was thought to be an emergency ATP synthesis system if oxidative phosphorylation and/or glycolytic ATP synthesis fail. PCr was proposed to be the major carrier for transport of "high-energy" phosphoryl groups in the cell between mitochondria and sites of ATP hydrolysis (5, 29, 41).

Figure 10 shows that CK activity reduces the amplitude of the oscillation in cytosolic ADP concentration, by ~60% for a V_{CK} change from 0.02 to 1. The oscillation in ATP synthesis is reduced even more. The P_i oscillation is virtually unaltered, because it is not buffered by the CK reaction. However, the P_i concentration is decreased from ~2.1 mM for $V_{CK} = 0.02$ to ~1.55 mM for $V_{CK} = 1$. Damping the ADP oscillation and decreasing the P_i concentration in the cytosol by CK activity is of importance to muscle cell function, because these breakdown products of the myosin ATPase might inhibit contractile function.

The contribution of PCr to transport of "high-energy" phosphate groups is only 32% at an ATP hydrolysis rate of 486.5 $\mu M\ s^{-1}$ for the rabbit heart parameters, which is modest. However, this contribution depends on the parameters chosen: it becomes 72% for the rat heart parameters and becomes 88% if the CK activity is further increased by threefold relative to the "rat heart" reference condition. The contribution of PCr to high-energy phosphate transport determined in the present study is somewhat lower than predicted in other models (29).

Conclusion. A model for the adenine nucleotide-creatine phosphate module in the metabolic system was derived by selecting key processes involved in the fast regulation of oxidative phosphorylation and in transfer of high-energy phosphoryl groups. This model explains measurements on the fast regulation of oxidative phosphorylation in isolated hearts with glycolysis inactivated. The addition of a glycolytic module will be necessary to explain the slower regulation of oxidative phosphorylation in vivo with glycolysis active. The advantage of the "skeleton model" approach is that compact modules are tested while detail and size of the model are kept to a minimum. The model predicts results of experimental interventions useful for further tests, and can be easily incorporated in larger models because it is compact. The model demonstrates effective buffering of metabolite oscillations, reduction of the peak value of ADP and reduction of the average value of P_i by CK activity.

APPENDIX A

Equations for the adenine nucleotide-creatine-phosphate module. Here the model equations used for the simulation of the adenine nucleotide-creatine-phosphate (ACP) module are described. The ACP module exchanges ADP and P_i from the IMS for ATP with a module representing mitochondrial ATP production. ATP is split to ADP and P_i in the cytosol by an ATP hydrolysis module. The ACP module therefore exchanges metabolites with two other modules whose simple representation is also described below.

A glossary of the variables in the model, which are dynamically changing during a simulation run, is given in Table 1. The subscript ims denotes the concentrations in the IMS, the subscript cyt denotes the concentrations in the cytosol (see Fig. 1). The parameters in the model, which are kept constant during a simulation run, are summarized in Table 2. The time derivatives of the concentrations (C) of five metabolites (ATP, ADP, PCr, Cr, and P_i) are calculated, each for two compartments: the cytosol and the intermembrane space (IMS):

$$dC_{ATP,cyt}/dt = (-J_{hyd} - J_{CK,MM} + J_{diff,ATP})/V_{cyt} \quad (A1)$$

$$dC_{ADP,cyt}/dt = (J_{hyd} + J_{CK,MM} + J_{diff,ADP})/V_{cyt} \quad (A2)$$

$$dC_{PCr,cyt}/dt = (J_{CK,MM} + J_{diff,PCr})/V_{cyt} \quad (A3)$$

$$dC_{Cr,cyt}/dt = (-J_{CK,MM} + J_{diff,Cr})/V_{cyt} \quad (A4)$$

$$dC_{Pi,cyt}/dt = (J_{hyd} + J_{diff,Pi})/V_{cyt} \quad (A5)$$

Table 1. *Variables in the model of the adenine nucleotide-creatine-phosphate module*

Variable	Description	Start Value at 135 beats/min
	Concentrations	
$C_{ATP,cyt}$	ATP concentration in cytosol	5,601 μM
$C_{ADP,cyt}$	ADP concentration in cytosol	64 μM
$C_{PCr,cyt}$	PCr concentration in cytosol	5,710 μM
$C_{Cr,cyt}$	Cr concentration in cytosol	9,790 μM
$C_{Pi,cyt}$	P_i concentration in cytosol	912 μM
$C_{ATP,ims}$	ATP concentration in IMS	5,626 μM
$C_{ADP,ims}$	ADP concentration in IMS	39 μM
$C_{PCr,ims}$	PCr concentration in IMS	5,711 μM
$C_{Cr,ims}$	Cr concentration in IMS	9,789 μM
$C_{Pi,ims}$	P_i concentration in IMS	910 μM
	Chemical conversions (expressed per unit volume of total intracellular water)	
J_{hyd}	ATP hydrolysis in cytosol	
J_{syn}	ATP production, i.e., flux of ATP entering the IMS from the mitochondrial matrix via the adenine nucleotide translocator	
$J_{CK,MM}$	rate of PCr production via muscle isoform of CK in cytosol	
$J_{CK,Mi}$	rate of PCr production via mitochondrial isoform of CK in IMS	
	Transport fluxes (expressed per unit volume of total intracellular water)	
$J_{diff,ATP}$	diffusion flux of ATP from IMS to cytosol	
$J_{diff,ADP}$	diffusion flux of ADP from IMS to cytosol	
$J_{diff,PCr}$	diffusion flux of PCr from IMS to cytosol	
$J_{diff,Cr}$	diffusion flux of Cr from IMS to cytosol	
$J_{diff,Pi}$	diffusion flux of P_i from IMS to cytosol	

Start value refers to ATP hydrolysis rate = 486.5 μM/s. These values are time averaged over the cardiac cycle. For the rabbit heart parameter set, see Table 2. Cyt, Cytosol; ims, intermembrane space.

$$dC_{ATP,ims}/dt = (J_{syn} - J_{CK,Mi} - J_{diff,ATP})/V_{ims} \quad (A6)$$

$$dC_{ADP,ims}/dt = (-J_{syn} + J_{CK,Mi} - J_{diff,ADP})/V_{ims} \quad (A7)$$

$$dC_{PCr,ims}/dt = (J_{CK,Mi} - J_{diff,PCr})/V_{ims} \quad (A8)$$

$$dC_{Cr,ims}/dt = (-J_{CK,Mi} - J_{diff,Cr})/V_{ims} \quad (A9)$$

$$dC_{Pi,ims}/dt = (-J_{syn} - J_{diff,Pi})/V_{ims} \quad (A10)$$

where J_{syn}, J_{hyd}, $J_{CK,MM}$, and $J_{CK,Mi}$ are the reaction rates per unit volume of total intracellular water of ATP synthesis, ATP hydrolysis, net rate of the MM-CK reaction, and net rate of the Mi-CK reaction. $J_{diff,Met}$ denotes the transport fluxes between the IMS and cytosolic compartments (Met denoting the metabolite involved; positive numbers indicate net diffusion fluxes going from IMS to cytosol). V_{ims} and V_{cyt} are the volumes of the IMS and cytosolic compartments, respectively, given as fraction of the total intracellular water volume. Reaction and diffusion rates are expressed per unit volume of total cell water, rather than per unit volume of the specific compartment, to make them directly comparable between cell compartments. Because the concentrations in the *Eqs. A1–A10* above are expressed in amount per unit volume of the specific compartment, the summed rates are divided by the fractional volumes, V_{ims} and V_{cyt}, yielding a correct mass balance in each compartment. Note that the mitochondrial matrix volume is not part of the ACP module.

The CK reaction rate J_{CK} is described by the following equation from Ref. 33, which describes a sequential, rapid equilibrium, random bi-bi enzymatic reaction mechanism that corresponds well with experimental data on the CK enzymes (33, 34)

$$J_{CK,iso} = [V_{max,iso,f} \cdot C_{ATP,comp} \cdot C_{Cr,comp}/(K_{ia,iso}K_{b,iso}) - V_{max,iso,b} \cdot C_{ADP,comp} \cdot C_{PCr,comp}/(K_{ic,iso}K_{d,iso})]/DenCK \quad (A11)$$

with

$$DenCK = 1 + C_{Cr,comp}/K_{ib,iso} + C_{PCr,comp}/K_{id,iso} + C_{ATP,comp}[1/K_{ia,iso} + C_{Cr,comp}/(K_{ia,iso}K_{b,iso})] + C_{ADP,comp}[1/K_{ic,iso} + C_{PCr,comp}/(K_{id,iso}K_{c,iso}) + C_{Cr,comp}/(K_{ic,iso}K_{lb,iso})] \quad (A12)$$

where the compartment indicator *cyt* or *ims* is substituted for *comp* for the MM-CK and Mi-CK reactions, respectively, and the isoform MM or Mi is substituted for *iso*. This reflects that the Mi-CK reaction is located in the IMS compartment and the MM-CK reaction in the cytosol (Fig. 1). The reaction rate is counted positive in the direction of PCr formation.

Equations A11 and *A12* govern the rates of both $J_{CK,Mi}$ and $J_{CK,MM}$ with separate kinetic constants for the mitochondrial or MM isoenzyme, respectively; see Table 2. Please note that the kinetic equations for the CK reactions reproduce extensive measurements on the isolated enzymes very well, both for the MM-CK (34) and Mi-CK (21, 33) isoforms.

The cytosolic and IMS compartments are separated by a partly permeable diffusion barrier formed by MOM. Metabolites permeating the outer mitochondrial membrane, thereby leaving the IMS and entering the cytosolic space, are taken into account in the mass balances of the IMS and cytosol. Diffusional fluxes, J_{diff}, between the intermembrane space and the myofibrillar space across the MOM depend on the permeability surface product (PS), expressed per unit volume of total intracellular water to be consistent with the unit for fluxes (see above):

$$J_{diff,ATP} = PS_{tot,ATP} \cdot (C_{ATP,ims} - C_{ATP,cyt}) \quad (A13)$$

$$J_{diff,ADP} = PS_{tot,ADP} \cdot (C_{ADP,ims} - C_{ADPcyt}) \quad (A14)$$

$$J_{diff,PCr} = PS_{tot,PCr} \cdot (C_{PCr,ims} - C_{PCr,cyt}) \quad (A15)$$

$$J_{diff,Cr} = PS_{tot,Cr} \cdot (C_{Cr,ims} - C_{Cr,cyt}) \quad (A16)$$

$$J_{diff,Pi} = PS_{tot,Pi} \cdot (C_{Pi,ims} - C_{Pi,cyt}) \quad (A17)$$

where $PS_{tot,Met}$ is the conductance parameter for metabolite Met, calculated from the diffusion coefficient in the cytosol and the MOM permeability (see APPENDIX B). By definition, the positive direction of flux is from IMS to cytosol. Although these diffusion equations are strictly speaking applicable to a steady state, the radial diffusion times in cytosol and intermembrane space are very small relative to the total delay in the system (see APPENDIX B). The situation is similar to the analysis of a resistor capacitance circuit in electrical engineering: the electrical current and potential across the resistor adapt so quickly to changing electrical potential at the capacitor that the steady-state equation of Ohm's law, electrical potential difference equals resistance times electrical current, is used to model the contribution of the resistor to the transient. The very small time delays across the resistor are neglected. Likewise, in models of vascular transport and permeation into the interstitial space, this type of steady-state equation involving the permeability-surface product of the blood vessel is used and radial diffusion times can often be neglected (3).

The metabolites obey the following moiety conservation relations:

$$(C_{ATP,cyt} + C_{ADP,cyt}) \cdot V_{cyt} + (C_{ATP,ims} + C_{ADP,ims}) \cdot V_{ims} = C_{AdN,tot} \cdot (V_{cyt} + V_{ims}) \quad (A18)$$

$$(C_{PCr,cyt} + C_{Cr,cyt}) \cdot V_{cyt} + (C_{PCr,ims} + C_{Cr,ims}) \cdot V_{ims} = C_{Cr,tot} \cdot (V_{cyt} + V_{ims}) \quad (A19)$$

$$(C_{ATP,cyt} + C_{PCr,cyt} + C_{Pi,cyt}) \cdot V_{cyt} + (C_{ATP,ims} + C_{PCr,ims} + C_{Pi,ims}) \cdot V_{ims} = C_{Pi,tot} \cdot (V_{cyt} + V_{ims}) \quad (A20)$$

Table 2. *Parameter values for the adenine nucleotide-creatine-phosphate module and the ATP synthesis and hydrolysis modules*

Name	Description	Value and Unit	Reference No.
	Rabbit Parameter Set		
MiCK (parameters mitochondrial creatine kinase enzyme)			
$V_{max,Mi,f}$	maximum velocity in the forward direction (PCr production)	$8.82 \cdot 10^2$ μM/s	(17, 18)[a,b]
$V_{max,Mi,b}$	maximum velocity in the backward direction (ATP production)	$3.704 \cdot 10^3$ μM/s	(17, 18)[b]
$K_{ia,Mi}$	binary dissociation constant ATP	$7.5 \cdot 10^2$ μM	(2, 23)
$K_{ib,Mi}$	binary dissociation constant Cr	$2.88 \cdot 10^4$ μM	
$K_{ic,Mi}$	binary dissociation constant ADP	$2.048 \cdot 10^2$ μM	
$K_{id,Mi}$	binary dissociation constant PCr	$1.6 \cdot 10^3$ μM	
$K_{b,Mi}$	ternary dissociation constant Cr	$5.2 \cdot 10^3$ μM	
$K_{d,Mi}$	ternary dissociation constant PCr	$5.0 \cdot 10^2$ μM	
$K_{c,Mi}$	ternary dissociation constant ADP	$K_{ic,Mi} \cdot K_{d,Mi}/K_{id,Mi}$	
$K_{lb,Mi}$	ternary dissociation constant Cr from dead end complex	$K_{ib,Mi}$	
MMCK (parameters muscle creatine kinase enzyme in the cytosol)			
$V_{max,MM,f}$	maximum velocity in the forward direction (PCr production)	$1.144 \cdot 10^4$ μM/s	(17, 18)[a,c]
$V_{max,MM,b}$	maximum velocity in the backward direction (ATP production)	$4.804 \cdot 10^4$ μM/s	(17, 18)[c]
$K_{ia,MM}$	binary dissociation constant ATP	$9.0 \cdot 10^2$ μM	(2, 23)
$K_{ib,MM}$	binary dissociation constant Cr	$3.49 \cdot 10^4$ μM	
$K_{ic,MM}$	binary dissociation constant ADP	$2.224 \cdot 10^2$ μM	
$K_{id,MM}$	binary dissociation constant PCr	$4.73 \cdot 10^3$ μM	
$K_{b,MM}$	ternary dissociation constant Cr	$1.55 \cdot 10^4$ μM	
$K_{d,MM}$	ternary dissociation constant PCr	$1.67 \cdot 10^3$ μM	
$K_{c,MM}$	ternary dissociation constant ADP	$K_{ic,MM}K_{d,MM}/K_{id,MM}$	
$K_{lb,MM}$	ternary dissociation constant Cr for dead end complex	$K_{ib,MM}$	
Diffusional Conductance Cytosolic Compartment			
$PS_{diff,ATP}$	diffusional conductance ATP	2,208 s^{-1}	(11)
$PS_{diff,ADP}$	diffusional conductance ADP	2,167 s^{-1}	
$PS_{diff,PCr}$	diffusional conductance PCr	3,083 s^{-1}	
$PS_{diff,Cr}$	diffusional conductance Cr	3,792 s^{-1}	
$PS_{diff,Pi}$	diffusional conductance P_i	3,958 s^{-1}	
Outer Membrane Permeabilities with Restricted Adenine Nucleotide Transfer			
$PS_{mom,ATP}$	membrane conductance ATP	13.3 s^{-1}	optimized
$PS_{mom,ADP}$	membrane conductance ADP	13.3 s^{-1}	
$PS_{mom,PCr}$	membrane conductance PCr	162.5 s^{-1}	(41)
$PS_{mom,Cr}$	membrane conductance Cr	162.5 s^{-1}	
$PS_{mom,Pi}$	membrane conductance P_i	204.4 s^{-1}	
Fractional volumes			
V_{cyt}	cytosolic compartment volume (0.461 ml/g ww) as fraction of total intracellular water volume (0.615 ml/g ww)	3/4	(1, 35)[e]
V_{ims}	intermembrane space volume (0.038 ml/g ww) as fraction of total intracellular water volume	1/16	
Total metabolite contents			
$C_{AdN,tot}$	total adenine nucleotide content	$5.665 \cdot 10^3$ μM	(12, 13)
$C_{Cr,tot}$	total creatine content	$1.550 \cdot 10^4$ μM	
$C_{Pi,tot}$	total content phosphate groups	$1.2225 \cdot 10^4$ μM	
ATP synthesis			
$V_{max,syn}$	maximum ATP synthesis velocity	$1.504 \cdot 10^4$ μM/s	(12)[d]
K_{ADP}	apparent K_M mitochondria for ADP	25 μM	(19, 25)
K_{Pi}	apparent K_M mitochondria for P_i	$8.0 \cdot 10^2$ μM	(19, 23)
ATP hydrolysis			
$J_{hyd,basis}$	ATP hydrolysis at 135 beats/min averaged over cardiac cycle	$4.865 \cdot 10^2$ μM/s	(17, 18)
$J_{hyd,test}$	ATP hydrolysis at 220 beats/min averaged over cardiac cycle	$6.276 \cdot 10^2$ μM/s	(17, 18)
	Rat Heart Parameter Set		
Same as rabbit heart parameter set, except:			
$V_{max,Mi,f}$ (rat) = $3.01 \cdot V_{max,Mi,f}$ (rabbit)			
$V_{max,Mi,b}$ (rat) = $3.01 \cdot V_{max,Mi,b}$ (rabbit)			
$V_{max,MM,f}$ (rat) = $1.65 \cdot V_{max,MM,f}$ (rabbit)			

Continued

Table 2.—*Continued*

Name	Description	Value and Unit	Reference No.
$V_{max,MM,b}$ (rat) = 1.65·$V_{max,MM,b}$ (rabbit)			
$V_{max,syn}$ (rat) = 3.06·$V_{max,syn}$ (rabbit)			
$C_{AdN,tot}$ (rat) = 1.75·$C_{AdN,tot}$ (rabbit)			
$C_{Cr,tot}$ (rat) = 1.68·$C_{Cr,tot}$ (rabbit)			
$C_{Pi,tot}$ (rat) = 2.62·$C_{Pi,tot}$ (rabbit)			

Temperature = 37 °C. To convert experimentally measured rates, determined at T = 25°C, to T = 37°C the temperature coefficient Q_{10} = 2 was used. The V_{max} of MM-CK, Mi-CK, and of ATP synthesis, total metabolite contents, and ATP hydrolysis levels for basis and test conditions were measured in the experimental model simulated here. [a]Vb/Vf = 4.199 (2); [b]Mi-CK activity: 1.15 IU / mg mito prot at T = 25 °C, measured in our laboratory in the experimental model which is simulated here (17, 18). [c]MM-CK activity: 4.54 IU total CK activity, corrected for mitochondrial CK activity, measured in our laboratory in the experimental model which is simulated here (18). [d]Corresponds to 68 μmol/(g_{dw}·min) of maximal O2 consumption at T = 37 °C, determined from isolated rabbit heart mitochondria in our laboratory (12). [e]total intracellular water volume and distribution in heart tissue, see (1). Note that the mitochondrial matrix is not part of the ACP module.

with $C_{AdN,tot}$ the constant total adenine nucleotide content, $C_{Cr,tot}$ the constant total creatine content, and $C_{Pi,tot}$ the constant total content of phosphate groups which can be transferred in the biochemical reactions.

The ATP exiting the mitochondrial matrix enters the IMS and thus enters the ACP module in *Eq. A6* with flux J_{syn}. ADP and P_i is exchanged with the ATP production module, as shown in *Eqs. A6, A7,* and *A10*, respectively. Hydrolysis flux J_{hyd} gives the exchange with the ATP hydrolysis module in the cytosol in *Eqs. A1*, *A2*, and *A5*.

Simple representation of ATP hydrolysis module communicating with the ACP module. The equations above describe the ACP module proper. Although we concentrate on the analysis of this ACP module, it communicates with two adjacent modules, representing ATP consumption in the cytosol and mitochondrial ATP production, respectively. These contacts embed the ACP module in the complete system.

First, we will discuss the ATP hydrolysis module. ATP hydrolysis in the cytosolic compartment, J_{hyd}, is found in *Eqs. A1*, *A2*, and *A5* of the ACP module. ATP consumption can be very efficiently represented by the time course of ATP cleavage during steps in heart rate, derived from experimental measurements. ATP turnover in the steady state is stoichiometrically related to O_2 consumption (12). Measurements of the rate of heat release show a sharp peak because of ATP splitting during systole, while ATP splitting is minimal during diastole (45).

Part of the simulations is therefore run with a pulsatile ATP hydrolysis rate, peaking during systole, as forcing function. The mathematical expressions for time-dependent ATP hydrolysis were described previously (41). The ATP hydrolysis rate, $J_{hyd,}$ increases linearly during the first one-sixth of the cardiac cycle to peak value $H_{ATP(max)}$

$$J_{hyd} = H_{ATP(max)} \cdot t/t_{cycle} \cdot 6 \quad \text{for} \quad 0 < t < 1/6 \cdot t_{cycle} \qquad (A21)$$

Here t is the time from the start of a cycle and t_{cycle} the period of the cycle in seconds.

During the next sixth of the cardiac cycle, J_{hyd} decreases from $H_{ATP(max)}$ to zero

$$J_{hyd} = H_{ATP(max)} \cdot [1 - 6 \cdot (t/t_{cycle} - 1/6)] \quad \text{for} \quad 1/6\, t_{cycle} < t < 1/3 \cdot t_{cycle} \qquad (A22)$$

During diastole, i.e., the rest of the cardiac cycle:

$$J_{hyd} = 0 \quad \text{for} \quad 1/3 \cdot t_{cycle} < t < t_{cycle} \qquad (A23)$$

(see Fig. 2 for an example of this time course).

From the steady-state basal level of ATP hydrolysis ($J_{hyd,basis}$) derived from O_2 uptake measurements at 135 beats/min (17), at t = 0 a step is made in heart rate to 220 beats/min and ATP hydrolysis rate $J_{hyd,test}$; these values are averaged over the cardiac cycle. ATP hydrolysis is calculated from the steady-state O_2 consumption measured in the experiments in the author's laboratory which are simulated here (17), assuming 4.8 molecules of ATP synthesized per molecule of O_2 consumed, a value measured experimentally for heart muscle (22). $H_{ATP(max)} = 6\, J_{hyd,basis}$ for a heart rate of 135 beats/min and $H_{ATP(max)} = 6\, J_{hyd,test}$ for 220 beats/min, based on *Eqs. A21–A23*.

Simple representation of ATP production module communicating with the ACP module. ATP production consists of ATP synthesis (syn) in the mitochondrial matrix by oxidative phosphorylation followed by ATP export across the mitochondrial inner membrane into the IMS. ADP leaves the IMS in immediate exchange for ATP across the adenine nucleotide translocator in the mitochondrial inner membrane. P_i leaves the IMS via the phosphate carrier across the mitochondrial inner membrane. The stoichiometry of oxidative phosphorylation dictates that for each molecule of ATP transferred from matrix to IMS, one molecule of ADP and one of P_i are transferred in the reverse direction, reflected by J_{syn} in *Eqs. A6*, *A7*, and *A10*. The ACP module therefore exchanges ADP and P_i for ATP with a module representing mitochondrial ATP production.

Oxidative phosphorylation and metabolism in the mitochondrial matrix are complex processes requiring a separate model which merits extensive analysis. Several such models have been devised and analyzed (4, 10, 26, 27). To focus the present study on the "skeleton model" of the ACP module, we do not analyze the applicability to rabbit cardiomyocytes of various competing complex models of the mitochondria and oxidative phosphorylation. Instead the communication between ACP module and ATP production module is represented by a simple Michaelis-Menten-type equation (*Eq. A24*). The ATP transfer rate, J_{syn}, from the mitochondrial matrix into the IMS is determined by a Michaelis-Menten-type equation depending only on ADP_{ims} and Pi_{ims}:

$$J_{syn} = V_{max,syn}(C_{ADP,ims} \cdot C_{Pi,ims})/(K_{Pi} \cdot K_{ADP} \cdot Den_{syn}) \qquad (A24)$$

with

$$Den_{syn} = 1 + C_{ADP,ims}/K_{ADP} + C_{Pi,ims}/K_{Pi} + C_{ADP,ims} \cdot C_{Pi,ims}/(K_{ADP} \cdot K_{Pi}) \qquad (A25)$$

This reflects ATP synthesis as measured in experiments on isolated mitochondria. The crucial point is that this equation has been experimentally validated (16, 36). It was also used in other models, see for instance (19, 25). The ATP amount transferred per unit time from the ATP production module to the ACP module is therefore completely determined by the ADP and P_i concentrations in the IMS in this model. Under stress conditions (hypoxia, low carbon substrate supply, presence of uncoupling substances) the parameters of *Eq. A24* may be affected because ATP synthesis also depends on the energization state of the mitochondria reflected in the mitochondrial membrane potential (27, 43). However, for the present study it is assumed that mitochondrial energization is not compromised, e.g., the heart is not ischemic or carbon substrate limited, and data on well-energized isolated mitochondria represented by *Eq. A24* are used. Because *Eq. A24* has

been well tested experimentally, it forms an efficient and simple representation of the ATP production module, adequate to test and investigate the ACP module. However, in future studies *Eq. A24* may be replaced by more complex computational modules for ATP production by the mitochondria.

APPENDIX B

Estimation of diffusion and membrane permeation parameters. The ACP module uses estimates of conductance parameters reflecting diffusion in the myofibrillar and cytosolic spaces and permeation of the MOM. Transport across the MOM is represented by the permeability-surface product PS. Because the diffusional conductance parameter for the cytosolic space is expressed in the same physical units, PS is used here also with subscript "diff ".

PS_{diff} is calculated from diffusion coefficients measured from diffusion-sensitized NMR spectra in muscle (11). The myofibril and its small surrounding cytosolic space is approximated with a cylinder with radius $a = 1.2$ μm (29, 41). The solution for the concentration profile for a metabolite diffusing into this cylinder is (29)

$$C(r) = C(a) - (Q/4D)(a^2 - r^2) \qquad (B1)$$

where $C(a)$ is the metabolite concentration at the outer surface of the cylinder with radius a and $C(r)$ is the concentration at distance r from the cylinder's axis. Q reflects the net chemical consumption of the metabolite diffusing into the cylinder per unit of volume in the cylinder. D is the diffusion coefficient of the metabolite. The average concentration difference between the cylinder's outer surface and the myofibrillar space follows by integration over the cylindrical space

$$\overline{C(r)} - C(a) = -(Qa^2/8D) \qquad (B2)$$

with the overbar denoting the spatial average.

J_{diff} of the metabolite, which balances the consumption rate Q, is expressed as

$$J_{diff} = PS_{diff} \cdot (C_a - \overline{C_{myofibril}}) \qquad (B3)$$

with PS_{diff} indicating the diffusional conductance in the cytosol (see Table 2). The Q value in *Eq. B1* is expressed per unit of intramyofibrillar volume, but the J_{diff} value is expressed in the model per unit volume of intracellular water (see APPENDIX A) to make metabolic rates and diffusional fluxes directly comparable between the compartments. *Equations B2* and *B3* give the following:

$$PS_{diff} = (8DV_{cyt})/a^2 \qquad (B4)$$

The diffusion coefficients for ATP and ADP were taken from ^{31}P-NMR diffusion spectroscopy in rat muscle (11): $D_{ATP} = 0.53\ 10^{-9}$ m^2/s and $D_{ADP} = 0.52\ 10^{-9}$ m^2/s. Based on these values, $PS_{diff,ATP} = 2{,}208\ s^{-1}$ and $PS_{diff,ADP} = 2{,}167\ s^{-1}$. From $D_{PCr} = 0.74\ 10^{-9}$ m^2/s and $D_{Cr} = 0.91\ 10^{-9}$ m^2/s it follows that $PS_{diff,PCr} = 3{,}083\ s^{-1}$ and $PS_{diff,Cr} = 3{,}792\ s^{-1}$. From $D_{Pi} = 0.95\ 10^{-9}$ m^2/s follows $PS_{diff,Pi} = 3{,}958\ s^{-1}$. If further hindrance to permeate the MOM is assumed to be negligible, this set of PS values constitutes parameter set I for total transport conductance.

The average diffusional transit time t_{diff} for a metabolite is defined by analogy to the mean transit time for a metabolized indicator, which was shown to equal the change in amount of metabolite in the system divided by the change in metabolic rate (40):

$$t_{diff} = \frac{-\Delta\overline{C(r)}}{\Delta Q} = \frac{a^2}{8D} \qquad (B5)$$

This t_{diff} for the cytosolic space is for ATP 0.340 ms, for ADP 0.346 ms, for PCr 0.243 ms, for Cr 0.197 ms and for P_i 0.189 ms. Diffusional transit times in the intermembrane space are smaller than in the myofibrillar space. The diffusion times in cytosol and intermembrane space (tenths of milliseconds) are so small relative to the total response time of oxidative phosphorylation (several seconds) that diffusional delays and gradients can be neglected. The diffusion gradients in the cytosol during the cardiac cycle were extensively modelled in (41) and shown to be very small.

Parameter PS_{diff} only takes diffusion through the myofibril and cytosol into account. However, the outer mitochondrial membrane is interposed between cytosol and IMS and its permeability is sometimes considered to be a major limiting factor (41). The permeation flux across the MOM is given by

$$J = PS_{mom} \cdot (C_{ims} - C_a) \qquad (B6)$$

The permeability coefficient P for ADP and ATP is assumed to be 0.16 μm/s in the model of Vendelin et al. (41). The conductance of the MOM, PS_{mom}, is then calculated to be 0.10 s^{-1} for ADP and ATP, taking the dimensions of the model into account (41). The total conductance, PS_{tot}, between myofibril and intermembrane space via cytosol and outer mitochondrial membrane is given by $1/(PS)_{tot} = 1/(PS)_{diff} + 1/(PS)_{mom}$, which is 0.099995 s^{-1} for ADP and ATP. For PCr and Cr the outer membrane permeability coefficient is 260 μm/s, yielding $PS_{mom} = 162.5$ and $PS_{tot} = 155\ s^{-1}$; for P_i with permeability coefficient 327 μm/s, $PS_{mom} = 204.4\ s^{-1}$ and $PS_{tot} = 194\ s^{-1}$. This set of PS_{tot} values constitutes parameter set II reflecting low MOM permeability for ADP and ATP.

Beard uses the same permeability coefficients (4), except for ADP and ATP where 85 μm/s is taken from measurements on isolated mitochondria (28). This results in $PS_{mom} = 53.1\ s^{-1}$ and $PS_{tot} = 51.9\ s^{-1}$. This set of PS values constitutes parameter set III.

In a later experimental study on permeabilized fibers (32), the permeabilities in Ref. 41 were modified: diffusibility in the cytosol was estimated to be 6% of the previously assumed diffusibility, and membrane permeability P was 3% of previous values, the latter being 260 μm/s for PCr and Cr, 327 μm/s for P_i and 145 μm/s for ADP and ATP. These values were thought to explain the experimentally determined ADP affinity of the mitochondria in permeabilized fibers. This results in the following parameter set: $PS_{tot,ATP} = PS_{tot,ADP} = 2.6\ s^{-1}$, $PS_{tot,PCr} = PS_{tot,Cr} = 4.6\ s^{-1}$ and $PS_{tot,Pi} = 5.8\ s^{-1}$. This is parameter set IV.

Finally, optimization to obtain correspondence with the measured response time of 3.7 s yielded 13.3 s^{-1} for PS_{tot} for ADP and ATP (see RESULTS), keeping the other PS values the same as in parameter sets II and III. This is parameter set V.

ACKNOWLEDGMENTS

The author is very grateful to Dr. O. Kongas for work on an early version of the model and for valuable advice.

GRANTS

The Centre for Medical Systems Biology is supported by a Genomics Centre of Excellence Grant from the Netherlands Genomics Initiative, which is funded by the Dutch government.

REFERENCES

1. **Aliev MK, Dos Santos P, Hoerter JA, Soboll S, Tikhonov AN, Saks VA.** Water content and its intracellular distribution in intact and saline perfused rat hearts revisited. *Cardiovasc Res* 53: 48–58, 2002.
2. **Aliev MK, Saks VA.** Compartmentalized energy transfer in cardiomyocytes: use of mathematical modeling for analysis of in vivo regulation of respiration. *Biophys J* 73: 428–445, 1997.
3. **Bassingthwaighte JB, Goresky CA.** Modeling in the analysis of solute and water exchange in the microvasculature. In: *The Handbook of Physiology. The Cardiovascular System. Microcirculation*. Bethesda, MD: Am. Physiol. Soc., 1984, sect. 2, vol. IV, pt. 1, chapt. 13, p. 549.
4. **Beard DA.** A biophysical model of the mitochondrial respiratory system and oxidative phosphorylation. *PLoS Comput Biol* 1: e36, 2005.
5. **Bessman SP, Geiger PJ.** Transport of energy in muscle: the phosphorylcreatine shuttle. *Science* 211: 448–452, 1981.

6. **Blasius B, Huppert A, Stone L.** Complex dynamics and phase synchronization in spatially extended ecological systems. *Nature* 399: 354–359, 1999.
7. **Brandes R, Bers DM.** Simultaneous measurements of mitochondrial NADH and Ca^{2+} during increased work in intact rat heart trabeculae. *Biophys J* 83: 587–604, 2002.
8. **Byrd R, Lu P, Nocedal J, Zhu C.** A limited memory algorithm for bound constrained optimization. *SIAM J Sci Comput* 16: 1190–1208, 1995.
9. **Chance B.** The energy-linked reaction of calcium with mitochondria. *J Biol Chem* 240: 2729–2748, 1965.
10. **Cortassa S, Aon MA, Marban E, Winslow RL, O'Rourke B.** An integrated model of cardiac mitochondrial energy metabolism and calcium dynamics. *Biophys J* 84: 2734–2755, 2003.
11. **de Graaf RA, van Kranenburg A, Nicolay K.** In vivo ^{31}P-NMR diffusion spectroscopy of ATP and phosphocreatine in rat skeletal muscle. *Biophys J* 78: 1657–1664, 2000.
12. **de Groot B.** *The role of mitochondria and intracellular energy transfer in the pathogenesis of heart failure* (PhD Thesis). Amsterdam: Vrije Universiteit, 1999.
13. **Eijgelshoven MH, van Beek JHGM, Mottet I, Nederhoff MG, van Echteld CJA, Westerhof N.** Cardiac high-energy phosphates adapt faster than oxygen consumption to changes in heart rate. *Circ Res* 75: 751–759, 1994.
14. **Erickson-Viitanen S, Viitanen P, Geiger PJ, Yang WC, Bessman SP.** Compartmentation of mitochondrial creatine phosphokinase. I. Direct demonstration of compartmentation with the use of labeled precursors. *J Biol Chem* 257: 14395–14404, 1982.
15. **Gustafson LA, van Beek JHGM.** Activation time of myocardial oxidative phosphorylation in creatine kinase and adenylate kinase knockout mice. *Am J Physiol Heart Circ Physiol* 282: H2259–H2264, 2002.
16. **Gyulai L, Roth Z, Leigh JS Jr, Chance B.** Bioenergetic studies of mitochondrial oxidative phosphorylation using 31phosphorus NMR. *J Biol Chem* 260: 3947–3954, 1985.
17. **Harrison GJ, van Wijhe MH, de Groot B, Dijk FJ, Gustafson LA, van Beek JHGM.** Glycolytic buffering affects cardiac bioenergetic signaling and contractile reserve similar to creatine kinase. *Am J Physiol Heart Circ Physiol* 285: H883–H890, 2003.
18. **Harrison GJ, van Wijhe MH, de Groot B, Dijk FJ, van Beek JHGM.** CK inhibition accelerates transcytosolic energy signaling during rapid workload steps in isolated rabbit hearts. *Am J Physiol Heart Circ Physiol* 276: H134–H140, 1999.
19. **Heineman FW, Balaban RS.** Phosphorus-31 nuclear magnetic resonance analysis of transient changes of canine myocardial metabolism in vivo. *J Clin Invest* 85: 843–852, 1990.
20. **Ideker T, Thorsson V, Ranish JA, Christmas R, Buhler J, Eng JK, Bumgarner R, Goodlett DR, Aebersold R, Hood L.** Integrated genomic and proteomic analyses of a systematically perturbed metabolic network. *Science* 292: 929–934, 2001.
21. **Jacobus WE, Saks VA.** Creatine kinase of heart mitochondria: changes in its kinetic properties induced by coupling to oxidative phosphorylation. *Arch Biochem Biophys* 219: 167–178, 1982.
22. **Kingsley-Hickman PB, Sako EY, Mohanakrishnan P, Robitaille PM, From AH, Foker JE, Ugurbil K.** 31P NMR studies of ATP synthesis and hydrolysis kinetics in the intact myocardium. *Biochemistry* 26: 7501–7510, 1987.
23. **Kongas O, van Beek JHGM.** Creatine kinase in energy metabolic signaling in muscle. *2nd Int. Conf. Systems Biology (ICSB 2001), Los Angeles, CA*. Madison, WI: Omnipress, 2001, p. 198–207.
24. **Kongas O, Wagner MJ, ter Veld F, Nicolay K, van Beek JHGM, Krab K.** The mitochondrial outer membrane is not a major diffusion barrier for ADP in mouse heart skinned fibre bundles. *Pflügers Arch* 447: 840–844, 2004.
25. **Kongas O, Yuen TL, Wagner MJ, van Beek JHGM, Krab K.** High K_m of oxidative phosphorylation for ADP in skinned muscle fibers: where does it stem from? *Am J Physiol Cell Physiol* 283: C743–C751, 2002.
26. **Korzeniewski B, Froncisz W.** An extended dynamic model of oxidative phosphorylation. *Biochim Biophys Acta* 1060: 210–223, 1991.
27. **Korzeniewski B, Noma A, Matsuoka S.** Regulation of oxidative phosphorylation in intact mammalian heart in vivo. *Biophys Chem* 116: 145–157, 2005.
28. **Lee AC, Zizi M, Colombini M.** β-NADH decreases the permeability of the mitochondrial outer membrane to ADP by a factor of 6. *J Biol Chem* 269: 30974–30980, 1994.
29. **Meyer RA, Sweeney HL, Kushmerick MJ.** A simple analysis of the "phosphocreatine shuttle". *Am J Physiol Cell Physiol* 246: C365–C377, 1984.
30. **Petzold LR.** Automatic selection of methods for solving stiff and nonstiff systems of ordinary differential equations. *SIAM J Sci Stat Comput* 4: 136–148, 1983.
31. **Petzoldt T.** R as a simulation platform in ecological modeling. *R News* 3: 8–16, 2003.
32. **Saks V, Kuznetsov A, Andrienko T, Usson Y, Appaix F, Guerrero K, Kaambre T, Sikk P, Lemba M, Vendelin M.** Heterogeneity of ADP diffusion and regulation of respiration in cardiac cells. *Biophys J* 84: 3436–3456, 2003.
33. **Saks VA, Chernousova GB, Gukovsky DE, Smirnov VN, Chazov EI.** Studies of energy transport in heart cells. Mitochondrial isoenzyme of creatine phosphokinase: kinetic properties and regulatory action of Mg^{2+} ions. *Eur J Biochem* 57: 273–290, 1975.
34. **Saks VA, Chernousova GB, Vetter R, Smirnov VN, Chazov EI.** Kinetic properties and the functional role of particulate MM-isoenzyme of creatine phosphokinase bound to heart muscle myofibrils. *FEBS Lett* 62: 293–296, 1976.
35. **Smith HE, Page E.** Morphometry of rat heart mitochondrial subcompartments and membranes: application to myocardial cell atrophy after hypophysectomy. *J Ultrastruct Res* 55: 31–41, 1976.
36. **Stoner CD, Sirak HD.** Steady-state kinetics of the overall oxidative phosphorylation reaction in heart mitochondria. *J Bioenerg Biomembr* 11: 113–146, 1979.
37. **Team RDC.** *R: A Language and Environment for Statistical Computing*. Vienna, Austria: Foundation for Statistical Computing, 2006.
38. **van Beek JHGM.** Channeling the data flood: handling large-scale biomolecular measurements in silico. *Proc IEEE* 94: 692–709, 2006.
39. **van Beek JHGM, Tian X, Zuurbier CJ, de Groot B, van Echteld CJ, Eijgelshoven MH, Hak JB.** The dynamic regulation of myocardial oxidative phosphorylation: analysis of the response time of oxygen consumption. *Mol Cell Biochem* 184: 321–344, 1998.
40. **van Beek JHGM, Westerhof N.** Response time of cardiac mitochondrial oxygen consumption to heart rate steps. *Am J Physiol Heart Circ Physiol* 260: H613–H625, 1991.
41. **Vendelin M, Kongas O, Saks V.** Regulation of mitochondrial respiration in heart cells analyzed by reaction-diffusion model of energy transfer. *Am J Physiol Cell Physiol* 278: C747–C764, 2000.
42. **Zeleznikar RJ, Goldberg ND.** Kinetics and compartmentation of energy metabolism in intact skeletal muscle determined from 18O labeling of metabolite phosphoryls. *J Biol Chem* 266: 15110–15119, 1991.
43. **Zhou L, Stanley WC, Saidel GM, Yu X, Cabrera ME.** Regulation of lactate production at the onset of ischaemia is independent of mitochondrial NADH/NAD^+: insights from in silico studies. *J Physiol* 569: 925–937, 2005.
44. **Zimmer SD, Ugurbil K, Michurski SP, Mohanakrishnan P, Ulstad VK, Foker JE, From AH.** Alterations in oxidative function and respiratory regulation in the post-ischemic myocardium. *J Biol Chem* 264: 12402–12411, 1989.
45. **Zuurbier CJ, Mast F, Elzinga G, van Beek JHGM.** Mitochondrial function is not decreased in stunned papillary muscle at 20°C. *J Mol Cell Cardiol* 29: 347–355, 1997.
46. **Zuurbier CJ, van Beek JHGM.** Mitochondrial response to heart rate steps in isolated rabbit heart is slowed after myocardial stunning. *Circ Res* 81: 69–75, 1997.